Research paper

Determination of optimum organic Rankine cycle parameters and configuration for utilizing waste heat in the steel industry as a driver of receive osmosis system

Reza Jaafari, A.B. Rahimi *

Department of Mechanical Engineering, Ferdowsi University of Mashhad, P.O.B. 91775–1111, Mashhad, Iran

ABSTRACT

The existence of the waste heat from the exhaust of steel industry with the temperature of 227 °C and water evaporation in the cooling process, the limitation of the water sources with high quality, the sharp decline of the groundwater, and access to the saline water are the reasons to study and analyze the ORC-RO system in this paper. This investigation is based on energy analysis (1E), exergy analysis (2E), economic analysis (3E), and environmental impacts (4E). The environmental analysis is conducted considering three aspects: (1) The effects of the ORC system depending on the selection of the working fluid. (2) The impacts of RO system on the brine, which depends on the brine stream density (introduced by the non-dimensional function Ω), showing the span of the RO system brine dilution. (3) The decline in the removal of the groundwater happens when the fresh water increases. In this comparison, four types of cycles consist of basic configuration, basic configuration with recuperator, basic configuration with regenerative, and basic configuration with the combination of regenerative and recuperator are investigated. The trade-off between exergy and thermal efficiency parameters and TAC (total annual cost) are the reason for using the Genetic Algorithm (GA) as the optimization algorithm. The main optimization parameters are: (1) configuration of ORC, (2) the optimized design of RO system, (3) Rankine cycle working fluid based on thermal source, (4) membrane selection among company membranes DOW, (5) determining the approach and pinch temperatures of WHR for maximum recovery, according to the limitation of acid dew point. These parameters are obtained based on two objectives; reducing the price of produced water and increasing the system's exergy efficiency. Production of freshwater reduces water withdrawal from groundwater resources, and the working fluid with low ODP and GWP reduces the environmental impacts of the cycle. The results show that the cycle with basic configuration and the cycle with recuperator are the two optimum cycles in the Pareto curve. The working fluid R245ca (GWP = 640; ODP = 0) is chosen as optimum fluid in each of the two cycles. The exergy efficiency, total cost and Ω in basic cycle and the cycle with recuperator are 32.51%, 2.84 \$/m^3, 16.94% and 32.49%, 2.64 \$/m^3, 12.74% respectively. Also, the production of freshwater reduces 2.5% of water withdrawal from groundwater resources.

1. Introduction

Water-Energy Nexus is the fundamental issue in most heavy industries such as steel industry. The rate of the consumed water in steel industries is different based on the process. For processes that use electricity, coal, and coke, the consumption rate is 0.64–60.14 m^3/MWh, 1–1.8 m^3/ton, and 1–2.8 m^3/h, respectively (Gao et al., 2011; Yang et al., 2020c; Zuo et al., 2015, 2017; Xu et al., 2020; Yang et al., 2015; Ma et al., 0000; Xue et al., 2020; Jiang et al., 2018). The water consumption for steel production in China

is 7–8.3 m^3/ton for monumental steel industries and is estimated at 3–4.2 m^3/ton for other industries (Gu et al., 2015; Zhang et al., 2020a, 2019b; Sun et al., 2019b; Zhang et al., 2021; Li et al., 2021; Yang et al., 2020b,a; Du et al., 2021). The water consumption for steel industries in Iran for sponge iron is 1–1.8 m^3/ton and for steel production and rebar reaches 2.8 m^3/ton. The quality of water in steel industries is different based on the type of consumption in other parts, and the range of the quality of water is 5–1000 ppm.

The global energy demand will increase 40 percent from 2006 to 2030 (Li et al., 2016; Wang et al., 2021, 2020; Rostamijavanani et al., 2020, 2021; Abasi et al., 2020; Alshawish et al., 2020; Zhang et al., 2020c; Jung et al., 2020). The steel industry is one of the energy-consuming industries that allocate 4–5 percent

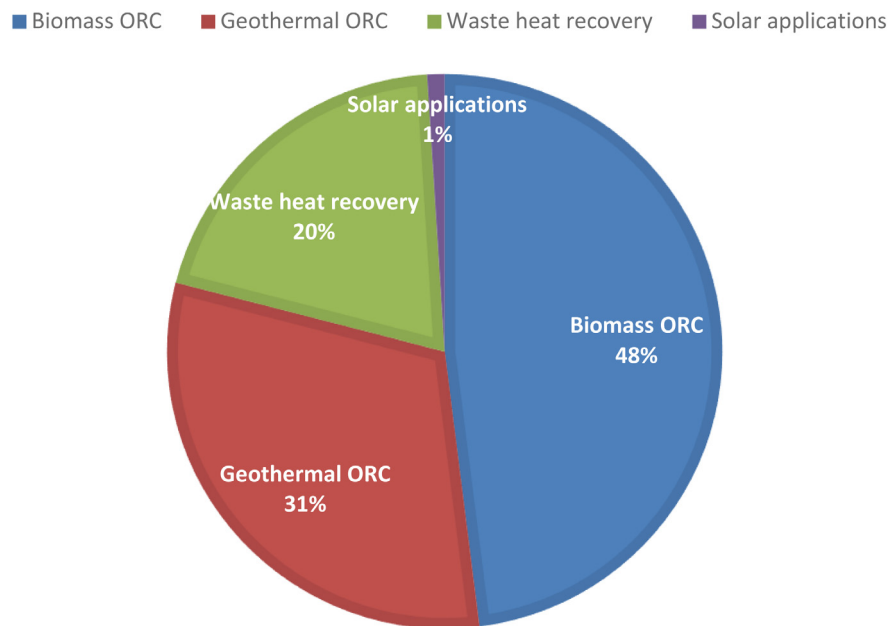■ Biomass ORC　■ Geothermal ORC　■ Waste heat recovery　■ Solar applications

Fig. 1. ORC shares in various low-grade thermal heat resources (Wei et al., 2007).

of global energy consumption (Yoon et al., 2020; Jafarishiadeh and Mohammadi, 2020; Davarpanah and Mirshekari, 2019; Hu et al., 2020b; Davarpanah, 2020, 2018; Razmjoo et al., 2020; Shirmohammadi et al., 2020a,b). In terms of the environment, this enterprise has a considerable share of global warming (Song et al., 2020; Ni et al., 2020; Wang and Jing, 2020; Guan and Jiang, 2020; Zhang and Zhao, 2020; Li, 2020; Venkateshkumar and Ramakrishnan, 2020; Huang, 2020). Based on the type of process, one ton of steel produces 1.9 tons of carbon dioxide (Zhu et al., 2020; Tang et al., 2020; Zhang et al., 2020d; Green, 2020). The average energy consumption for one ton of steel is 1.757 GJ. The steel industry is energy-consuming, and it is essential to reduce CO_2 propagation. These are several reasons why it is necessary to focus on thermal energy recovery procedures and reducing fuel consumption (Quader et al., 2015).

In Iran, despite benefiting from several non-petroleum mineral resources compared to the world extent (with coal 1%, ironstone 1.5%, lead and zinc 11%, copper 15% and chromite 8% of the entire world resources), the mineral base of economic growth is still negligible compared to the total economic development of the country. Hence, the steel industry has not been developed proportionally to the available resources. However, the steel industry uses nearly 22% of the total energy consumption of the major industries in Iran. In the study of energy audits carried out in the steel enterprise (rolling sheet production), the intensity of total energy consumed in the sample factory in Iran was 5.51 GJ/ton (Anon, 0000a). Improvement of thermal efficiency of systems, economic and environmental issues can be addressed in reducing steel industries energy consumption.

In this work, the authors attend the Basic Oxygen Furnace (BOF) type of furnaces and employ this type in assessments. The steelmaking enterprise should develop novel technologies for future energy conservation because of energy security, volatile and high energy prices, and climate changes. In this regard, waste heat recovery is one of the crucial technologies to obtain the requirements. To this end, exhaust gas should be introduced into successive heat exchangers to utilize the recycled heat in air and fuel (gas) preheat for combustion and contribution in the free-forming process. Consequently, the exhaust temperature approaches 200–300 °C.

The utilization of waste heat in addition to the efforts to benefit from the high penetration of renewable sources, were the initial motivations for using the Organic Rankine Cycle (ORC). The exclusive characteristics of fluid have made the ORC suitable for low-temperature heat recovery applications (generally under 400 °C). Fig. 1 represents ORC utilization shares in various low-grade thermal heat resources. As it is apparent, 20% of the resources are related to waste heat recovery (WHR). The research conducted by Modesto and Nebra (Modesto and Nebra, 2009) focused on waste energy (gas) recovery. In this research (Modesto and Nebra, 2009), a methodology was assessed for a power generation system based on the Rankine cycle and through Coke Oven Gas (COG) and Blast Furnace Gas (BFG). In this work, exergo-economic factors, cost variation, including relative cost variation, were computed to specify the effect of each component in the plant make-up cost and finding the most appropriate way for the generation cost of energy and process steam. A preventive method to improve the resilience of transmission system is introduced in Jafarishiadeh and Mohammadi (2020).

In Yao et al. (2013), an exergo-economic analysis was performed based on thermo-economics for a combined cycle system using associated gases (BFG, COG, and sintering waste gas) from the process of steel production. They also computed different exergo-economic indices such as exergo-economic factors, relative and absolute cost differences to analyze the exergo-economic performance of each piece of equipment. The effects of capital costs and decision variables on the momentary and unitary production costs were also investigated.

The parameters which are effective in the determination of enhancing ORC performance in WHR are as (1) The configuration of ORC; (2) Working fluid proportional to the conditions of heat resource; (3) High and low-temperature resources constraints (4) The purpose of using ORC for cogeneration. Various studies have been conducted on parameters such as working and configuration fluid based on heat sources. These researches are shown in Table 1.

In Kasaeian et al. (2018), the cogeneration system was studied. The authors analyzed the hybrid systems according to the solar energy for cogeneration of electricity and water. In El-Emam and Dincer (2018), a novel integrated solar-based system was studied and evaluated. The system was constructed from

Table 1
A review of recent papers regarding the decisive parameters to improve ORC performance.

Authors	Performance	Low temp	High temp	Utilized fluids	Case study cycle	Chosen fluids	Objective function
Badr et al. (1990)	WHR	30–50	120	R11, R113, R114	ORC	R113	–
Maizza and Maizza (2001)	–	35–60	80–110	Refrigerants	ORC	R123, R124	–
Liu et al. (2004)	WHR	30	150–200	R123, isoPentane, HFE7100, Benzene, Toluene, P-xylene	ORC	Benzene, Toluene, R123	–
Chammas and Clodic (2005)	ICE	55	150	Water, R123, isopentane, R245ca, R245fa, butane, isobutene, R-152a	ORC	Water, R245ca, isopentane	–
Drescher and Brüggemann (2007)	Biomass	90	250–350	ButylBenzene, Propylbenzene, Ethylbenzene, Toluene, OMTS	ORC	ButylBenzene	–
Hettiarachchi et al. (2007)	Geothermal	30	70–90	Ammonia, nPentane, R123, PF5050	ORC	Ammonia	**Capital Cost power plant**
Lemort et al. (2007)	WHR	35	60–100	R245fa, R123, R134a, nPentane	ORC	R123, nPentane	–
Saleh et al. (2007)	Geothermal	30	100	alkanes, fluorinated alkanes, ethers and fluorinated ethers	ORC	RE134, RE245, R600, R245fa, R245ca, R601	–
Borsukiewicz-Gozdur and Nowak (2007)	Geothermal	25	80–115	propylene, R227ea, RC318, R236fa, ibutane, R245fa	ORC	Propylene R227ea, R245fa	–
Mago et al. (2008)	WHR	25	100–210	R113, R123, R245ca, Isobutane	ORC; R_PRC	R113	–
Tchanche et al. (2009)	Solar	35	60–100	Refrigerants	ORC	R152a, R600, R600a R290, R134a	–
Façao et al. (2008)	Solar	45	120–230	Water, n-pentane HFE 7100, Cyclohexane, Toluene, R245fa, nDodecane, Isobutane	ORC, R_ORC	n-dodecane	–
Dai et al. (2009)	WHR	25	145	water, ammonia, butane, isobutene, R11, R123, R141b, R236ea, R245ca, R113	R_ORC, saturated/superheated, regenerative/non-regenerative, subcritical/supercritical	R236ea	–
Desai and Bandyopadhyay (2009)	WHR	40	120	Alcanes, Benzene, R113, R123, R141b, R236ea, R245ca, R245fa, R365mfc, Toluene	ORC, R_ORC	Toluene, Benzene	–
Chen et al. (2012)	WHR	50	80–220	R600a, R245fa, R123, R113	ORC, saturated/superheated	R113, R123	–
Mikielewicz and Mikielewicz (2010)	CHP	50	170	R365mfc, Heptane, Pentane, R12, R141b, Ethanol	ORC, ORC_R	Ethanol	–
Vaja and Gambarotta (2010)	ICE, WHR	35	95-221	R134a, R11, Benzene	double stage regenerated ORC system	Benzene	–
Aljundi (2011)	–	30	50–140	RC318, R227ea, R113, sobutene, nbutane, nhexane, isopentane, neopentane, R245fa, R236ea, C5F12, R236fa	ORC	nhexane	–
Wang et al. (2011)	WHR	27–87	327	R245fa, R245ca, R236ea, R141b, R123, R114, R113, R11, Butane	ORC	R11,R141b,R113,R123, R245fa, R245ca	–
Roy et al. (2011)	WHR	–	277	R12, R123, R134a, R717	ORC_SH	R123	–
Wang et al. (2013b)	Global	10–17	130	R134a	ORC	N/a	Exergy efficiency Overall capital cost
Wang et al. (2013)	Global	10–17	150	R123, R245fa, Icobutane	ORC	R123, R245fa	Net power output Surface areas of both the HRVG and condenser Ratio of net power output to overall heat transfer area
Wang et al. (2013a)	Solar	N/a	150	R245fa, R123, Isobutane, R134a	ORC_R	R123, R245fa	A daily average efficiency Modified system efficiency
Astolfi et al. (2014a)	Global	N/a	120–180	RC318, R227ea, C4F10, RC318, C4F10, R227ea, RC318, C4F10, R227ea	Single pressure level cycles in saturated/superheated, regenerative/non-regenerative, subcritical/supercritical	N/a	Second law efficiency
Astolfi et al. (2014b)	WHR	N/a	150	RC318, R227ea, C4F10, RC318, C4F10, R227ea, RC318, C4F10, R227ea	Single pressure level cycles in saturated/superheated, regenerative/non-regenerative, subcritical/supercritical	N/a	Second law efficiency Specific plant investment cost
Ayachi et al. (2014)	WHR	N/a	150–160	R125, R1234yf, R134a, R227ea, R235fa, R124, R235ea, Isobutane, Isobutene, n-butane, R245fa,	ORC. R_ORC		Mechanical power output
Imran et al. (2014)		N/a	N/a	R123, R11, R245fa, R141b, R134a	ORC, double stage regenerated ORC system, single stage regenerative ORC system	R245fa	Thermal efficiency Specific investment cost

Table 1 (continued).

Authors	Performance	Low temp	High temp	Utilized fluids	Case study cycle	Chosen fluids	Objective function
Song and Gu (2015)	WHR	N/a	110–230	Cyclohexane, Benzene, Toluene, R141b, R11	ORC	cyclohexane/R141b (0.5/0.5)	Net power output Thermal efficiency Total cost of equipments
Yang and Yeh (2015)	WHR	N/a	N/a	R1234yf,, R152a, R1234ze, R245fa	ORC	R245fa 9%	Net power output Thermal efficiency Total cost of equipments
Sadeghi et al. (2016)	Geothermal	25	100	R22M, R402A, R402B, R403B, R404A, R407A, R410A, R422A, R422D, R438A, R245fa	ORC	R407A	Net power output Turbine size parameter
Liu et al. (2017)	geothermal	30	80–95	R245fa, R123, R134a, R152a	ORC, ORC_SH, single stage regenerative ORC system	R123	Pure net power, thermal efficiency, exergy efficiency, components cost.
Karimi and Mansouri (2017)	geothermal	20	150	R600a, R152a, R11, R601a,R134a, R123	ORC, R_ORC and TSEORC	Refrigerants	Thermoeconomic
Zare (2015)	geothermal	20	160–170	Isobutane, n-pentane, R245fa and R152a	ORC, R-ORC	N/a	total product cost
Vivian et al. (2015)	Global	35	120, 150, 180	R218, R1234yf, R227ea, R1234ze, RC318, R236fa, Isobutane, FC87, Butane, R245fa, HFE7000, FC72, Isopentane, HFE7100, Pentane, Hexane, HMDS,	R_ORC, ORC	N/a	maximization of cycle efficiency or system power output/efficiency
Branchini et al. (2013)	Global	33	150–450	MDM, MD2M, MD3M, R134a, R245fa, isobutane, butane, isopentane, PP2, PP5, toluene, butane, p-xylene	ORC, ORC-R, SH, R_ORC-R, R_ORC-R_SH	400 °C: Toluene 200 °C: R245fa and butane	–
Camporeale et al. (2015)	biomass	40	260–270	MM, Toluene MDM, MD2M	Saturated cycle, SH, ORC	N/a	–
Lingfeng Shia et al. (2018)	WHR	N/a	N/a	R218, R145a, R125, R41,Teluene, D4, Cyclohexan	ORC	N/a	–
Mokhtari et al. (2016c)	Geothermal	40	157	R123, R134a, R22, R245fa, Water	ORC	R123	Exergy efficiency, cost of electricity

Basic organic Rankine cycle (ORC), regenerative organic Rankine cycle (R_ORC), two-stage evaporation organic Rankine cycle (TSEORC), the superheated cycle (SH), regenerative cycle recuperated and regenerative cycle (R_ORC-R), the recuperated, regenerative and superheated (R_ORC-R_SH).

ORC, absorption cooling system, electrolyzer, and desalination unit for poly-generation purposes. The application of the system was studied from different aspects of economic, energy, and exergy. By utilizing geothermal energy, the authors of Behnama et al. (2018) analyzed a tri-generation system including hot water, freshwater, and electricity. Researchers in Kianfard et al. (2018) utilized geothermal energy for multi-generation as well. This system consisted of an electricity generation unit using the protein-energy malnutrition (PEM) and ORC systems, freshwater according to the RO technology, and hydrogen. The analysis of economic and exergy results indicated that the ORC has an investment return of 5.6 years as well as maximum exergy destruction. In another study (Pethurajan et al., 2018), the configurations and applications of this cycle were investigated and compared, paying attention to the ORC extension. In Salimi and Amidpour (2017), the zeotropic mixture for the power generation system was optimized. Optimization results indicated the appropriate performance of systems with zeotropic mixture compared to those with pure fluid. In another research (Bao et al., 2018b), an internal combustion engine (ICE) for the production of freshwater was modeled. The results of this study showed that utilizing the waste heat and steam production of multiple-effect distillation (MED) system, 26.78 m3/d of freshwater is produced.

Eveloy et al. (2017) modeled the SOFC-GT+ORC-RO system (SOFC: Solid Oxide Fuel Cell, GT: Gas Turbine). The system was optimized based on the cost reduction and exergy efficiency increase. The results showed that the investment return was less than 6 years. Baccioli et al. (2018) modeled the ORC cycle with the MED. The superheated steam enters the ORC, and the heat is transferred to the system until the steam reaches the saturation temperature and then enters the MED. In other configurations of the ORC with recuperator, the outlet heat from the turbines enters the recuperator and preheats the inlet MED water. Lai et al. (2018) studied the Stirling engine connected to the RO system with and without the Energy recovery device (ERD). The maximum recovery was estimated equal to 17.3% for this system, and the amount of specific energy consumption (SEC) was SEC = 2,5 m^3/kWh.

Mokhtari et al. (2016a) studied Reverse Osmosis (RO) system in solar cycle combined with ORC. Firstly, the RO system was optimized by considering the constant demand. Afterward, for this RO system, the Rankine cycle with working fluids R717? R123? R290 and water were designed with the lowest cost in the cycle and solar farm. The results for working fluids demonstrated that the R123 had the lowest total annual cost (TAC). Li et al. (2013a) investigated research articles focusing on the RO+ORC system until 2013. The focus was on scenarios in which the output power of the turbine in ORC was the driver for the RO pump. In this study, various fluids were studied in the organic cycle combined with a solar farm in two scenarios, super-critical and sub-critical, of the cycle and based on economic and energy analysis. The results showed that at lower temperatures than 150 °C, the R245fa is able to produce more fresh water in the sub-critical system. Geng et al. (2016) studied ORC with RO for the zeotropic mixture. They achieved the highest power and freshwater production in a low-temperature thermal source. It was obtained by preheating water and a mixture of 0.9/0.1 from the working fluid type of R600/R601a. Delgado-Torres and García-Rodríguez (2010) studied the ORC connected to the solar farm. This system aimed to produce fresh water. They obtained the pump power in the RO system for two types of brackish water and seawater. They compared and analyzed isopentane, butane, R245ca, and R245fa as working fluids and finally selected R245fa as the working fluid of the cycle.

Table 2 is provided to review the novelties and contributions of the presented works. It can be seen that up to 88% of the articles used renewable energies to analyze the ORC-RO system. In this paper, the RO model is developed based on the exact model of mass transfer topics. In the ORC cycle section, which is the focus of this paper, four different cycles have been thoroughly

Table 2
Innovations of the present work compared to other articles.

Contributions of this paper	Description of the differences with other articles	References reviewed
Use of recycled heat to electricity production for the ORC-RO system	Over 88% of papers in this field have used solar energy to analyze the ORC-RO system.	Delgado-Torres and García-Rodríguez (2007a,b), García-Rodríguez and Delgado-Torres (2007), Manolakosa et al. (2007), Bruno et al. (2008), Manolakosa et al. (2008), Manolakos et al. (2009b,a), Kosmadakis et al. (2009b,a, 2010b), Tchanche et al. (2010), Nafey et al. (2010), Kosmadakis et al. (2010a), Karellas et al. (2011), Delgado-Torresa and Garcia-Rodriguez (2012), Peñate and García-Rodríguez (2012) and Li et al. (2013b)
RO model development	Mesh each membrane and solve the equations for each section and determine the output water quality based on mass transfer equations	Manolakosa et al. (2005), Delgado-Torres and García-Rodríguez (2007a,b), García-Rodríguez and Delgado-Torres (2007), Manolakosa et al. (2007), Nemati et al. (2017), Igobo and Davies (2018) and Arab Chadegania et al. (2018)
Considering the environmental impacts on the working fluid	Provide a working fluid algorithm based on the environmental analysis	Manolakosa et al. (2007), Bruno et al. (2008), Manolakosa et al. (2008), Manolakos et al. (2009a), Kosmadakis et al. (2010b), Delgado-Torresa and Garcia-Rodriguez (2012), Igobo and Davies (2018) and Arab Chadegania et al. (2018)
Sensitivity analysis on each aspect of the proposed ORC cycle	Detailed examination of each statue based on the proposal and its analysis	Manolakos et al. (2009b), Kosmadakis et al. (2009a), Nafey et al. (2010), Karellas et al. (2011), Delgado-Torresa and Garcia-Rodriguez (2012), Peñate and García-Rodríguez (2012) and Li et al. (2013b)
Use of wasted heat in the cycle to improve RO from an environmental perspective	The effect of heating water on produced fresh water and buoyancy force in its dilution	Mokhtari et al. (2016a) and Geng et al. (2016)
Consideration of case study limitations (steel plant)	The temperature of the exhaust smoke based on the amount of water is higher than the amount presented in other articles. The pressure drop in the smoke path should be within the compressor range of the process and should not lead to a change in path pressure.	Nemati et al. (2017) and Igobo and Davies (2018)
Multi-objective optimization	Determining 37 decision parameters using genetic algorithm (GA) based on water price reduction and exergy efficiency. Also, providing a decision curve based on optimal water price and exergy efficiency	Delgado-Torres and García-Rodríguez (2007a,b), García-Rodríguez and Delgado-Torres (2007), Manolakosa et al. (2007), Bruno et al. (2008), Manolakosa et al. (2008), Manolakos et al. (2009b,a), Kosmadakis et al. (2009b,a, 2010b), Tchanche et al. (2010), Nafey et al. (2010), Kosmadakis et al. (2010a), Karellas et al. (2011), Delgado-Torresa and Garcia-Rodriguez (2012), Peñate and García-Rodríguez (2012), Li et al. (2013b), Nemati et al. (2017), Igobo and Davies (2018) and Arab Chadegania et al. (2018)

studied along with conducting several sensitivity analyses, and finally, it has been optimized. Also, in this work, heat losses are used for the reduction of RO environmental impacts. In these studies, it is observed that only two articles have used heat losses. Also, the articles have briefly reviewed the various ORC configurations. Only two articles performed system optimization. This shows that the study of the ORC-RO system with water preheating can be interesting from the viewpoint of 4E and freshwater production.

Ehyaei et al. (2020) investigated the thermodynamic optimization of a geothermal plant using GA in two stages. In the first stage, the optimal variables of well depth and geothermal fluid extraction velocity were considered. By determining these values in the second stage, the geothermal power plant was optimized with the ORC cycle to achieve the maximum output power. Yousefizadeh Dibazar et al. (2020) performed experimental and exergy analysis on three different organic Rankine cycles.

In the following, the energy and exergy analysis and the advanced exergy analysis of these three cycles have been performed and compared. With a conventional exergy analysis, researchers can evaluate the performance of components separately to find the one with the highest amount of exergy destruction.

The advanced analysis divides the exergy destruction rate into unavoidable and avoidable and endogenous and exogenous parts.

The results showed that the priority of component improvement is by condensers and turbines, respectively.

Esfandi et al. (2020) analyzed energy, exergy, economics, and a new hybrid system for generating electricity and cooling. This solution has been considered to reduce the consumption of fossil fuels and alleviate environmental impacts. Hybrid systems generate electricity using the spectrum of solar radiation. The results showed that the energy and exergy efficiencies of this combined system are respectively 24.7% and 23%. The payback period of this system is 15.6 years. In addition, regarding the environmental impacts of CO_2, it is worthy of mentioning the recent investigations by Daryayehsalameh, who introduced new methods to absorb CO_2 (Daryayehsalameh et al., 2021).

Mehrpooya et al. (2018) evaluated the thermodynamics and economics of a concentrated solar system with absorption refrigeration and freshwater cycles.

In this study, an innovative concentrated solar power plant integrated with desalination process and absorption refrigeration cycle aimed at supplying power, freshwater, and refrigeration, was developed and exergetically assessed. The system comprised a concentrated solar thermal power plant with parabolic dish

collectors and steam turbine, a multi-effect desalination process with the parallel feed of seawater, and a single-stage ammonia–water absorption refrigeration system. Generally, the collectors provided 21,030 kW thermal power to the steam power plant, and 4632 kW was converted to electrical power in the steam power plant. The absorption refrigeration cycle produced 820.8 kW refrigeration, and the desalination cycle provided fresh water at a rate of 22.79 kg/s.

In another analysis, Mehrpooya et al. (2019) evaluated the performance of a biogas system by solar panel collectors under the Kalina cycle.

This study aims to develop and introduce a novel integrated system composed of a water scrubbing biogas upgrading process with water regeneration, flat plate solar collectors (FPC), and Kalina power cycle. Solar thermal energy was exploited by means of FPCs and delivered to the Kalina cycle aiming at producing the electrical power required by the biogas upgrading process. The excess heat in the biogas upgrading cycle was recovered and fed to the Kalina cycle. The proposed system was simulated by Aspen Hysys based on the actual solar data for Bushehr city. Overall, the FPCs provided 2627 kW thermal power to the Kalina cycle, where 289.5 kW electrical power was produced and delivered to the biogas upgrading process.

The results show that the integrated efficiency of this system is 92.36%, and the highest external degradation is related to FPC.

In this paper, various configurations of ORC according to energy (1E), exergy (2E), economic (3E), and environmental analysis (4E) were studied to provide the power of RO for high-pressure pumps. The main reasons for utilizing GA to select the cycle and working fluid configuration were the increase in the costs by applying some components such as heat exchangers and recuperator in the cycles case study and the changes in efficiency and power in these types of cycles. Freshwater production was considered in the optimization process to supply a part of the water needed for the cycle. The important reasons for applying GA for RO configuration selection and design with energy recovery device (ERD) were the variety of membranes and associated costs and the design of RO configuration.

In this paper, according to the case study, which is a steel plant, there are various limitations that have significant impacts on the optimization constraints and especially on selecting the ORC cycle. Among them, the high percentage of H_2O and CO_2 can be mentioned. By decreasing the temperature from 130 degrees, they lead to the dew point and the production of carbonic acid. As a result, failure in the ORC cycle evaporator tube is inevitable.

The pressure drop on the gas side of the combustion products should not exceed the range specified for the compressor (0.2 bar). This will reduce the flow of the compressor and affect the process and disrupt production (Han and Li. H. Feng. Y. Tian. Z. Jiang. Tong He, 2021; Yoon and Ahn, 2021; Lu et al., 2021; Chao. K. Zhang et al., 2018; Zhang et al., 2019c; Liu et al., 2020; Niu et al., 2020; Zhang et al., 2020b).

One of the major contributions of the present work is to conduct sensitivity analysis on all the studied cycles. The studied cycles are not compared with each other, and the role of working fluid change on the cycle and target functions is not specified. This paper has tried to determine the effect of each aspect and working fluid change on the target functions simultaneously by examining each cycle separately.

In this paper, by considering the impact of recovery on total cost, the effect of these two indicators on working fluid in different parts of the ORC cycle has been investigated. Additionally, this paper has tried to determine the main indicators in an ORC-RO cycle that use heat recovery are affected by analyzing the cases.

Also, the results of sensitivity analysis (the impact of recovery on total cost) indicated that it is not necessary to consider recovery in the environmental function, which has been considered in the mentioned paper. The authors of Daryayehsalameh et al. (2021) have not considered the effect of density ratios, which is the main factor for the buoyancy force and system dilution. Also, it is not affected by the recovery. They evaluated the role of preheating in freshwater production and final concentration only by using heat losses. This would cause the optimization with the price indicator in the recovery to automatically affect the volume size. The only effective factor in reducing the environmental impacts is the density ratio.

In the mentioned paper, based on ODP and GWP, fluids were predetermined for competition. However, using the algorithm presented in this paper, fluids with the above environmental indicators were also proposed to determine them based on the constraints and objective functions of the genetic algorithm.

In general, this paper tries to take a deeper look at the new 4E + D problem considering different aspects of the ORC cycle and the working fluid by sensitivity analysis and examine the 4E characteristics in the selected cycle more closely.

By reviewing the literature review, the novelties of the current research are as follows:

1- The selection of the optimum parameters of the ORC-RO system from 4E perspective and preheating of the inlet water by using the waste heat source of the factory (the case study: steel industry)

2- The membrane selection and desalination stages by GA in ORC-RO cycle, determination of the A_w and B parameters for 23 membranes of the DOW company.

3- Optimization of freshwater production by the ultimate goal of decline in groundwater withdrawal and environmental impacts of RO system brine.

4- Introducing the non-dimensional parameter Ω for demonstrating the environmental impacts of the RO waste, which indicates a decline in dilution span.

5- Determination of the optimum parameters of the ORC-RO cycle based on the GA for seawater desalination.

2. System description

The waste heat in the steel industry and the evaporation of water in the cooling process, the limitation of the water sources with suitable quality, the sharp decline of the groundwater, and having access to the saline water were the reasons to analyze the ORC-RO combined system. Fig. 2 shows the schematics of the steel industry process with 800 ton/h productions. According to this figure, the combustion products from the furnace are used for preheating process of air and natural gas after being washed to reduce their temperature. This paper focuses on the outlet of the heat exchanger (HEX), which is being sent toward the chimney of the factory with a mass flow rate of 75 kg/s and a temperature of 272 °C (Zhang et al., 2019a). By considering the system's operation by a pressure lower than air pressure, the exhaust fume exits from the system by fans. The schematic of the case study cycles is demonstrated in Fig. 3. Each cycle consists of two parts: electricity generation and desalinated water production. In the power production cycle, it is necessary to mention that the base cycle of ORC is Cycle A (Hu et al., 2020c, 0000, 2020a, 2021).

In Fig. 3, the cycle with recuperator is Cycle B, which is put in the primary cycle. In order to determine this configuration, it is necessary to consider turbine outlet conditions according to the working fluid (dry) (Yang et al., 2021). The organic fluid preheating causes pinch temperature determination in WHR based on inlet conditions (In cold stream: working fluid of ORC. In hot stream: combustion products with constant temperature). An appropriate pinch temperature selection leads to a rise in thermal recovery. The heat exchanger is added to the organic Rankine
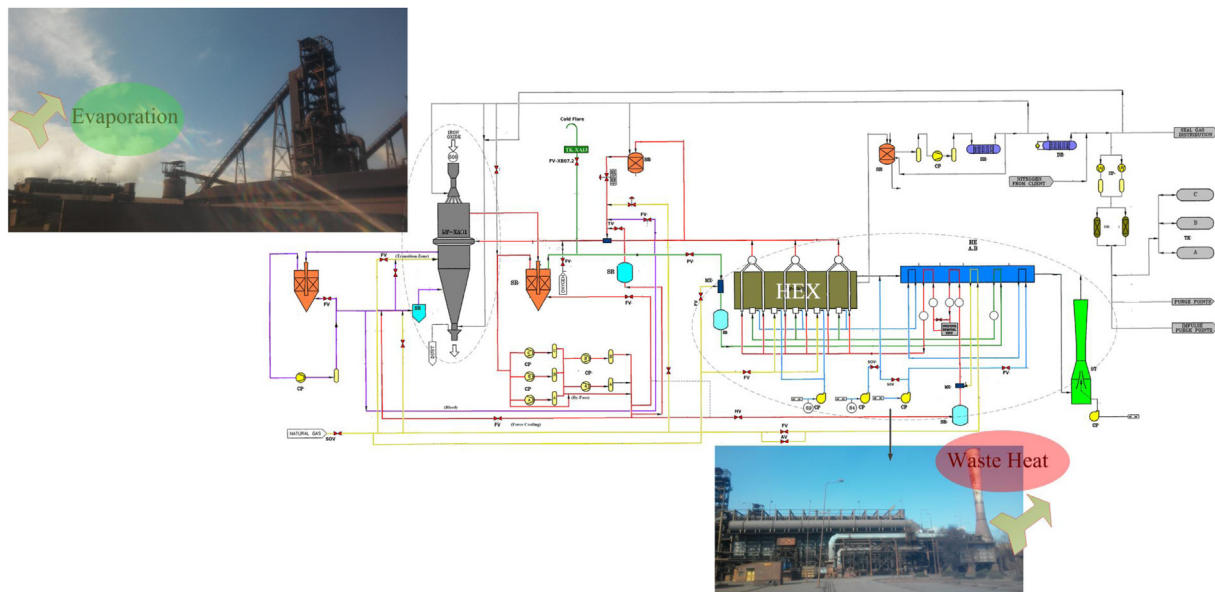
Fig. 2. Schematics of the steel industry production process and demonstration of the heat recovery potential and losses of water from wet cooling towers.

Cycle C, which gets the working fluid from turbine and causes heating of organic fluid, enhancing the cycle's efficiency. In Fig. 3, the recuperator with a heat exchanger is put in ORC (Cycle D). This increases the fluid inlet temperature to WHR (Jiang et al., 2021). As a result, more percentage of energy gives rise to more generation of turbine inlet working fluid, instead of raising the temperature of the cold stream. Determining the flow rate of this cycle is also according to the approach and pinch temperatures of WHR. Adding a component to a cycle, in addition to efficiency improvement and net power increase/reduction, rises the costs of that cycle (Zhang et al., 0000b).

3. Methodology

In this paper, the ORC-RO system is considered in terms of 4E since the available and important indexes of the system are introduced one by one.

– *The energy and exergy analysis (1E & 2E)*

The modeling of the four configurations of the ORC based on the mentioned relations is performed at the first step. Each cycle is modeled individually and can be coupled to the other systems by optimizing each configuration. By selecting the key parameters in these systems like the turbine inlet fluid pressure, the condenser temperature, the extractions pressure, and the pinch and approach temperatures in WHR, the modeling and determination of the exergy thermal efficiencies index's modeling and determination ORC is done. The RO+ERD design is done so that the GA determines the number of RO stages, pressure vessels (PVs) based on recovery, membranes in each PV, and the type of the membranes of the DOW company according to the defined goals. The exergy efficiency can be increased, and the SEC index is decreased by utilizing the ERD system. The exergy analysis of the RO streams is done considering the changes in salt density.

– *Economic analysis (3E)*

Determining each parameter in the energy analysis section affects the total cost of freshwater and electricity. The thermodynamic parameters affect the cycle costs based on the chosen function. Ultimately, the ORC thermodynamic changes and RO system results can be seen in the total cost. The considered costs are O&M and capital costs. The O&M costs for the RO system are the cost of the chemical additive for pretreatment, the membrane change costs, the cost of the equipment for withdrawal of the water from the sea, and the laboratory costs to maintain the inlet and outlet water conditions (Duan. B. Deng et al., 2021).

– *The analysis of environmental impacts (4E)*

The environmental impacts are divided into three categories in this paper: (1) the effects of the ORC system selection, which depending on the fluid and is introduced by the ozone depleting potential (ODP) and global warming potential (GWP) indexes. (2) The RO brine effects depend on the brine stream density, which is shown Ω in this paper (the non-dimensional function that demonstrates a decline in the RO system brine dilution). (3) The decline in the water withdrawal happens when the produced freshwater increases. Due to utilizing a wet cooling tower in the process and wasting water during evaporation, there is a need to use procedures for decreasing the withdrawal of water wells. The freshwater production from the available saline water sources causes a decline in the withdrawal of groundwaters (Lv et al., 2021, 0000; Yu, 2021; Ji et al., 2021; Hou et al., 2021; Ji et al., 2020).

The purpose of the designed system is to decrease the net price of produced water and system exergy efficiency increase. The net price decline happens with water production increase and system costs decrease. The increase in the system's exergy efficiency is also with the exergy destruction decrease. Based on each of the analyses, each parameter has a specific impact on the desired goals. Fig. 3 indicates that how the indexes of the ORC and RO are related. Fig. 4 also shows the role of each cycle parameter on the analysis and the indexes of the ORC-RO.

In the section on power generation (ORC), the trade-off between these four cycles in thermal and net power, exergy efficiency, and TAC must be analyzed in the form of the final purpose of the freshwater production system. In the section on the freshwater configuration, selecting the number of stages is one of the parameters that should be determined according to the system conditions (Ji et al., 0000).

The water enters the ORC condenser from the sea, and the temperature rises in this section. The outlet water from the condenser has two positive impacts on the RO system. Firstly,
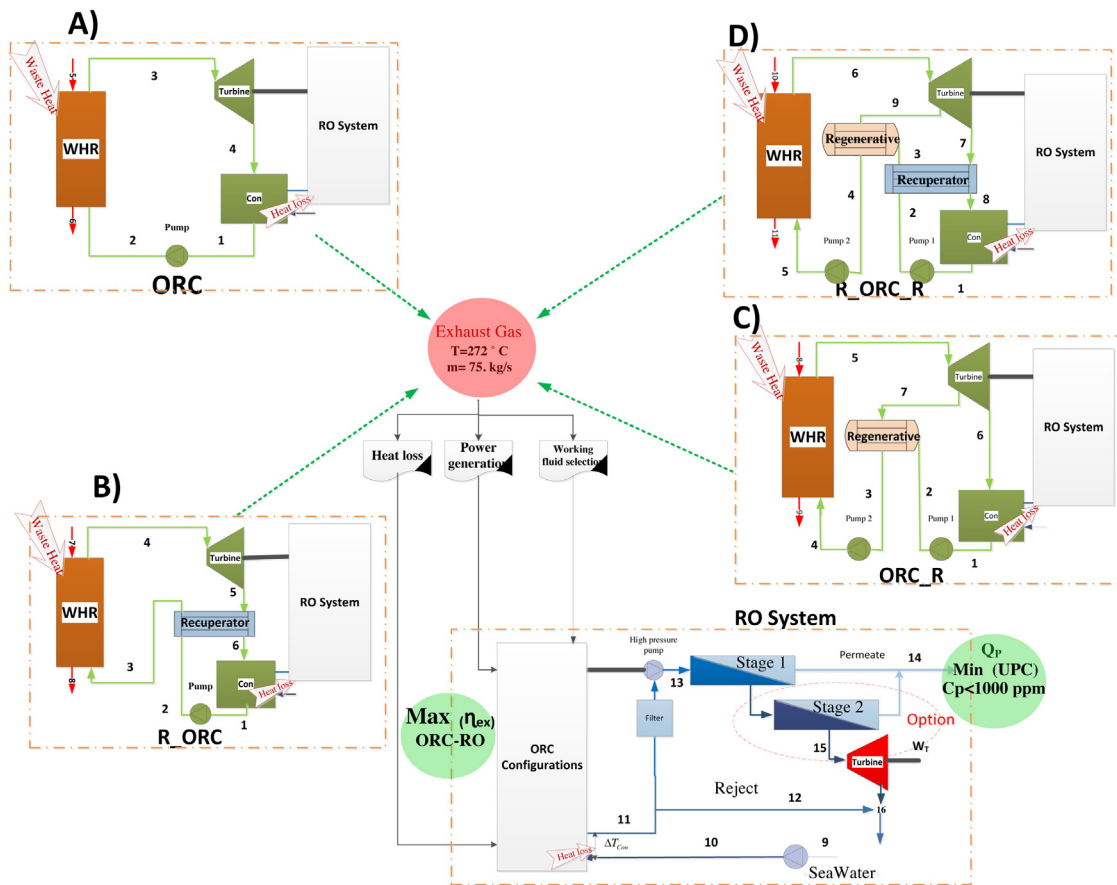
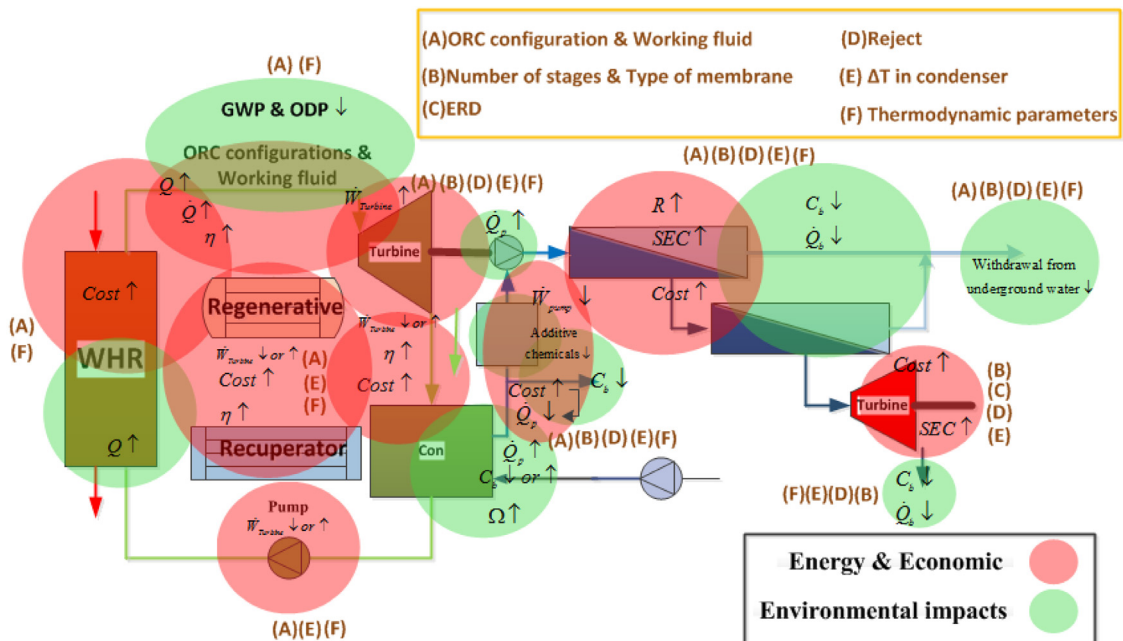**Fig. 3.** Schematics of the ORC and RO connection.

Fig. 4. Schematics of the impact of each parameter on others from the energy, economic and environmental perspectives and the domain of parameters impact.

it reduces the intake costs; secondly, it improves the conditions of freshwater production rate (Mokhtari et al., 2016a). There would be several merits in the co-location of a power plant and a desalination plant by considering concentrate disposal point of view. The merits could be cost reductions in sharing an outfall structure and the concentrate dilution to amend its compatibility with the receiving water. The environmental impacts of high saline discharge are minimized when the discharge concentration is decreased. The discharge salinity may be as low as the natural variation in seawater; hence, this lower discharge of saline

Table 3

The first and second law of thermodynamic equations and the functions of each component price Mokhtari et al. (2016a), Bejan and Moran (1996), Ameri et al. (2008), Peng et al. (2021), Sun et al. (2019a), Zhang et al. (0000a), Kordestani et al. (2021), Dong et al. (2021), Hua et al. (2021) and Cai et al..

Component	Inlet parameters	Energy relation	Exergy relation	Capital cost (CC)
Turbine	η_T P_6	$T_6 \langle K \rangle = T_{sat}(P_6)$ $\eta_T = \dfrac{h_6 - h_8}{h_6 - h_{8,is}}$ $W\left\langle \dfrac{kJ}{kg} \right\rangle = m_7(h_6 - h_7) + (1 - m_7)(h_6 - h_8)$ $\dot{W}_T \langle kW \rangle = \dot{m}_7(h_6 - h_7) +$ $\dot{m}_8(h_6 - h_8)$	$\dot{Ex}_D = \dot{Ex}_6 - \dot{Ex}_7 - \dot{Ex}_8 - \dot{W}_T$ $\dot{Ex}_F = \dot{Ex}_6 - \dot{Ex}_7 - \dot{Ex}_8 \dot{Ex}_P = \dot{W}_T$ $\eta_{Ex} = \dfrac{\dot{Ex}_P}{\dot{Ex}_F} \rightarrow$ $\eta_{Ex} = \dfrac{\dot{W}_T}{\dot{Ex}_6 - \dot{Ex}_7 - \dot{Ex}_8}$	$CC_T = 3880.5 \dot{W}_T^{0.7} \phi_\eta \phi_T$ $\phi_\eta = \left(1 + \left(\dfrac{1 - 0.95}{1 - \eta_T}\right)\right)^4$ $\phi_T = \left(1 + 5\left(\exp\left(\dfrac{T_6 - 866}{10.42}\right)\right)\right)$
Internal Heat Exchanger (IHE)/Recuperator	η_{IHE}	$\eta_{IHE} = \dfrac{T_8 - T_9}{T_8 - T_1}$ $A_{IHE} \langle m^2 \rangle = \dfrac{\dot{Q}_{IHE}}{U \times \Delta T_{LM}}$	$\dot{Ex}_D = (\dot{Ex}_8 + \dot{Ex}_2)$ $- (\dot{Ex}_9 + \dot{Ex}_3)$ $\dot{Ex}_F = \dot{Ex}_3 - \dot{Ex}_2$ $\dot{Ex}_P = \dot{Ex}_8 - \dot{Ex}_9$ $\eta_{Ex} = \dfrac{\dot{Ex}_8 - \dot{Ex}_9}{\dot{Ex}_3 - \dot{Ex}_2}$	$CC_{IHE} = 8000 + 259.2 \times A_{IHE}^{0.91}$
Condenser	T_1 ΔT	$P_1 = P_{sat}(T_{con})$ $\dot{Q}_{cond} \langle W \rangle = \dot{m}_1(h_9 - h_1)$ $T_{cw,o} = T_{cw,i} + \Delta T$ $T_{cw,i} = T_{sw}$ $\dot{m}_w\left\langle \dfrac{kg}{s} \right\rangle = \dfrac{\dot{Q}_{cond}}{Cp_w \Delta T}$	$\dot{Ex}_D = (\dot{Ex}_9 + \dot{Ex}_{W,i}) -$ $(\dot{Ex}_1 + \dot{Ex}_{W,o})$ $\dot{Ex}_F = \dot{Ex}_{W,i} - \dot{Ex}_{W,o}$ $\dot{Ex}_P = \dot{Ex}_9 - \dot{Ex}_1$ $\eta_{Ex} = \dfrac{\dot{Ex}_9 - \dot{Ex}_1}{\dot{Ex}_{W,i} - \dot{Ex}_{W,out}}$	$CC_{cond} = \dfrac{280.74 \dot{Q}_{cond}}{2200 \Delta T} + 746 \dot{m}_W$ $+ 70.5 \dot{Q}_{cond} \times$ $\left(-0.6936 \ln\left(T_{cw,o} - T_{cw,i}\right) + 2.1897\right)$
Pump 1	η_P P_7	$h_2 = h_1 + W_P\left\langle \dfrac{kJ}{kg} \right\rangle$ $W_P\left\langle \dfrac{kJ}{kg} \right\rangle = \dfrac{(P_2 - P_1)}{\eta_P \rho_1}$ $P_2 = P_7$ $\dot{W}_{p,1} \langle kW \rangle = \dot{m}_1(h_2 - h_1)$	$\dot{Ex}_D = (\dot{W}_P + \dot{Ex}_1) - \dot{Ex}_2$ $\dot{Ex}_F = \dot{W}_P$ $\dot{Ex}_P = \dot{Ex}_2 - \dot{Ex}_1$ $\eta_{Ex} = \dfrac{\dot{Ex}_2 - \dot{Ex}_1}{\dot{W}_P}$	$CC_p = 549.13(W_P)^{0.71} f_m \cdot \phi_\eta$ $\phi_\eta = 1 + \left(\dfrac{1 - 0.8}{1 - \eta_1}\right)^3$ $f_m = \begin{cases} \text{cast iron} = 1 \\ \text{Steel} = 1.41 \end{cases}$ f_m: **Material correction factor, here:** $f_m = 1.41$
Open feed-organic heater (OFOH)	P_7	$\varepsilon = \dfrac{\dot{Q}}{\dot{Q}_{max}}$ $T_7 = f(P_7, h_7)$	$\dot{Ex}_D = (\dot{Ex}_7 + \dot{Ex}_3) - \dot{Ex}_4$ $\dot{Ex}_F = \dot{Ex}_7 + \dot{Ex}_2$ $\dot{Ex}_P = \dot{Ex}_4$ $\eta_{Ex} = \dfrac{\dot{Ex}_2 - \dot{Ex}_1}{\dot{W}_P}$	$CC_{OFOH} = b\left(\dot{Q}_{OFOH}\right)^{0.7}$ $b = 145.315 \dfrac{\$}{kW^{0.7}}$
WHR	T_{app} $T_{p.p}$ $T_{G,i}$ $\dot{m}_G$ $\bar{X}_G$	$T_{app} = T_{sat} - T_{f,o,Eco}$ $T_{p.p} = T_{G,o,Eva} - T_{sat}$ $Eco: \dot{m}_G Cp_G (T_{G,i,Eco} - T_{G,o,Eco}) =$ $\dot{m}_f (h_{f,o,Eco} - h_{f,i,Eco})$ $Eva: \dot{m}_G Cp_G (T_{G,i,Eva} - T_{G,o,Eva}) =$ $\dot{m}_f (h_g - h_{f,o,Eco})$ $Cp_G = f(\bar{X}_G, T_G)$	$\dot{Ex}_D = (\dot{Ex}_{G,in} + \dot{Ex}_6) -$ $(\dot{Ex}_{G,out} + \dot{Ex}_5)$ $\dot{Ex}_F = \dot{Ex}_{G,i} - \dot{Ex}_{G,o}$ $\dot{Ex}_P = \dot{Ex}_6 - \dot{Ex}_5$ $\eta_{Ex} = \dfrac{\dot{Ex}_6 - \dot{Ex}_5}{\dot{Ex}_{G,i} - \dot{Ex}_{G,o}}$	$CC_{HRSG} = c\left[\left(\dfrac{\dot{Q}_{Eco}}{\Delta T_{LM,Eco}}\right)^{0.8} + \left(\dfrac{\dot{Q}_{Eva}}{\Delta T_{LM,Eva}}\right)^{0.8}\right] +$ $d \times \dot{m}_{ORC} + e \times \dot{m}_G^{1.2}$ $c = 6570 \dfrac{\$}{(kW/K)^{0.8}}$ $d = 21276 \dfrac{\$}{(kg/s)}$ $e = 1184.4 \dfrac{\$}{(kg/s)^{1.2}}$

The inlet constant parameters in this table are as follow: $\eta_T = 80\%$, $\eta_{IHE} = 80\%$, $\eta_P = 85\%$, $T_{G,i} = 272\ °C$, $\dot{m}_G = 75$ kg s and $\bar{X}_G$ is demonstrated in molar compounds percentage in Table 6.

needs a less complex diffuser design and a shorter outfall. In addition, the dense, negatively buoyant concentrate is considered by the warm, positively buoyant power plant discharges, further rising the concentrate compatibility. This decreases mixing zone extent as well as the amount of time required for proper dilution and mixing. Such a process finally alleviates environmental impacts (Ehyaei et al., 2020). According to (1) the condition and quality of process water, (2) the pressure required for feed water in RO, (3) the ORC net power conditions and (4) reaching the higher the costs of fewer chemicals injection a recovery of RO system, the outlet reject water form condenser is determined. (Fig. 3 Cycle A stream 10). After passing through filter and pretreatment and injection of chemicals, the seawater enters the RO system high-pressure pump. The high-pressure pump delivers all the net power of the ORC and is designed according to the maximum generation and minimum water cost. The diversity of DOW membranes complicates selecting the membrane. Nevertheless, companies have various procedures to select the membrane (Ladewig and Asquith, 2012; Anon, 0000b). The

membrane selection for raw water coming from the sea is not exclusive. This selection among different membranes according to the raw water condition and economics and exergy problems is one of the matters studied in the RO section.

The trade-off among different cycles and electricity delivery to RO system for producing freshwater according to configuration system has to be optimized as well as the pressure vessel (PV) design based on the number, recovery, and type of membranes from exergy and economic perspective. The more freshwater, the less water withdrawal from underground water, which reduces the environmental impacts. The rise in water production has a direct effect on reducing the environmental impacts. Besides, the working fluid selection reduces the environmental index like Ozone depletion potential (ODP) and global warming potential (GWP). These are the objectives of optimization. According to current conditions and for the optimum mode, the cycle is proposed for the steel factory, which can (1) obtain a desirable amount for mentioned parameters and (2) design the RO configuration with the minimum cost of freshwater. Fig. 4 illustrates the connection between the parameters of energy, cost, and environmental

Table 4
The information of the ORC-RO.

Parameters	Unit	Value	Description
Turbine inlet fluid pressure	kPa	2500	Cycle A to D
Condenser temperature	°C	43	Cycle A to D
Turbine extraction pressure	kPa	1000	Cycle C and D
Pinch temperature	°C	60	Cycle A to D
Approach temperature	°C	7	Cycle A to D
Number of RO stages	–	2	Cycle A to D
Type of first stage membrane	–	SW30HRLE-370 34i	Cycle A to D
Type of second stage membrane	–	BW30HR-440i	Cycle A to D
Number of membranes in each PV	–	5	Cycle A to D
Temperature difference between inlet and outlet water (Condenser)	°C	10	Cycle A to D
The amount of water rejection	%	30	Cycle A to D

impacts. This figure determines the effect of each parameter on other parameters and the extent of the affective domain.

4. Modeling

4.1. Energy analysis

• *The ORC modeling*

Energy, exergy, and economic relations of Cycle D (illustrated in Fig. 3), shown in Table 3. Different cycles are modeled similarly to this cycle and based on their components. One can find the modeling of other cycles in reference Safarian and Aramoun (2015).

Net power parameter is determined in the turbine modeling according to the inputs of isentropic efficiencies, condenser temperature (condenser pressure), and input pressure (saturation temperature). Net mass flow of cycle enters the turbine. As a result, inlet mass flow to the turbine is taken into account, and the other mass flows are measured accordingly. WHR equations are used for determining the cycle mass flow.

There are four unknown parameters in WHR equations. These parameters are $\dot{m}_f$, $T_{f,o,Eco}$, $T_{G,i,Eco}$, and $T_{G,o,Eco}$ which are respectively the mass flow of fluid circulating in ORC, the temperature of feed water from economizer, the inlet and outlet temperatures of economizer gasses. When mass flow is obtained from the equations, it is viable to calculate the output power and heat rate for each component of Table 3 according to the continuity equations.

The unknowns can be determined in the heat exchangers based on the thermal efficiency (ε, η_{IHE}), performance factor, and performance conditions. For example, the organic fluid has to be on the saturation line at the outlet in the hot stream side of IHE. In the condenser, the inlet water temperature is assumed to be equal to the temperature of the sea. Also, the temperature of the outlet water of the condenser is obtained according to the predefined temperature difference between the outlet and inlet waters. For computing the pump outlet temperature and enthalpy, it is possible to calculate the work per kilogram by having the pump's inlet and outlet temperatures. By summing the work per kilogram to the enthalpy, the unknowns are determined. The computation of some parameters is according to the cost function, and the amount of that should be computed based on thermodynamic characteristics such as heat transfer surfaces. The exergy equations are represented according to the fuel exergy, exergy destruction, product exergy definitions, and the exergy efficiency is introduced and computed according to the mentioned equations. These definitions as well as the equations of exergy balance, are described in the section of exergy analysis (2E).

The stack gas temperature should not be less than 125 °C due to the high percentage H₂O (Ganapathy, 2003; Mokhtari et al., 2016b). This issue helps prevent acid dew point corrosion in economizer tubes. The quality of working fluid at turbine exhaust is always more than 88% due to the chosen fluids, and so this matter has no restrictions for turbine (Ameri et al., 2018). The inlet parameters for simulation of the Cycles A to B are shown in Table 4.

• *The RO modeling*

RO system modeling is based on the correlation of each membrane element. This method makes it possible to achieve a more accurate model of the RO system with fewer assumptions (Mokhtari et al., 2016a; Anon, 0000b; Khanarmuei et al., 2017; Mokhtari et al., 2016d). For each element, the equations presented in Table 5 are solved.

According to the determination of the inlet pressure of the presented nonlinear equations, the water mass flux (J_w), salt mass flux (J_s), and based on the water velocity between the membrane layers (V_w), the concentration of water produced (C_p), the concentration of water on the wall (C_w), and finally the flow rate of condensed and produced water is determined. Each membrane is divided into 70 finer elements to minimize the error in the calculations (Mokhtari et al., 2016a). In addition to the main equations, the auxiliary equations are used to determine the mass transfer coefficient (k), the Reynolds number (R_e) based on the velocity V_w of the pressure drop across the membrane, the osmotic pressure (π), and the temperature correction factor (Du et al., 2014; Al-Bastaki and Abbas, 2000). Considering the temperature change and its effect on C_p and Q_p parameters, the proposed equation for DOW membranes is as follows (Mokhtari et al., 2016a):

$$TCF = EXP\left[2640(\frac{1}{298} - \frac{1}{273 + T_f})\right], \quad T_f \geq 25\,^\circ C$$

$$TCF = EXP\left[3020(\frac{1}{298} - \frac{1}{273 + T_f})\right], \quad T_f \leq 25\,^\circ C \tag{9}$$

Table 5
Basic modeling equations for a RO element (Mokhtari et al., 2016a).

Equation	
$J_w = A_w \times TCF \left[\left(P_f - P_p - \frac{\Delta P_f}{2} \right) - \left(\pi_w - \pi_p \right) \right] \times 10^6$	(1)
$J_s = B \left(C_w - C_p \right)$	(2)
$V_w = \frac{J_w + J_s}{\rho_p}$	(3)
$C_p = \frac{J_s}{V_w} \times 1000$	(4)
$C_w = C_p + \left(\frac{C_f + C_b}{2} - C_p \right) e^{\frac{V_w}{k}}$	(5)
$Q_p = V_w S_m$	(6)
$Q_B = Q_F - Q_P$	(7)
$C_B = \frac{Q_F C_F - Q_P C_P}{Q_B}$	(8)

4.2. Exergy analysis (2E)

Based on the first law of thermodynamics and thermodynamic parameters, the exergy values can be calculated for each section. The exergy flow rate consists of chemical and physical rates, and other exergies such as potential and kinetic are ignored. Hence, the exergy flow rate is achieved as follows (Eveloy et al., 2017):

$$\dot{Ex} = \dot{Ex}^{PH} + \dot{Ex}^{CH} \quad (10)$$

Blast furnace combustion products and physical exergy for organic fluid can be described as Eq. (11) (Eveloy et al., 2017):

$$ex_{ph} = (h - h_\circ) - T_\circ(s - s_\circ); \quad \dot{Ex}^{PH} = \dot{m} \times ex_{ph} \quad (11)$$

Entropy and enthalpy can be calculated using (12) and (13) for every portion of blast furnace combustion products. Afterward, the total entropy and enthalpy can be computed based on equations represented for gas mixtures (Bejan and Moran, 1996):

$$S_i = \frac{1}{M_i} \left[S^+ + a \ln T + by - \frac{c}{2} y^{-2} + \frac{d}{2} y^2 - \bar{R} \ln \left(\frac{P_i}{P_{ref}} \right) \right] \quad (12)$$

$$h_i = \frac{10^3}{M_i} \left[H^+ + ay + \frac{b}{2} y^2 - cy^{-1} + \frac{d}{2} y^3 \right] \quad (13)$$

In which $y = 10^{-3}T$ is the reference environment pressure (1 atm), P_{ref} is constant numbers belonging to Eqs. (12) and (13) mentioned in Bejan and Moran (1996).

The calculation of chemical exergy, according to the flow type and chemical exergy of blast furnace combustion products and seawater, is described differently as below.

The chemical exergy of blast furnace combustion products can be associated with the percent of their components presented in Table 6. Chemical exergy can be calculated as (14), knowing the chemical exergy of each component (Bejan and Moran, 1996).

$$ex_{mix}^{ch} = \left[\sum_{i=1}^{N} x_i ex^{ch_i} + RT_0 \sum_{i=1}^{N} x_i ln x_i + G^E \right] \quad (14)$$

where i presents each component, x indicates the molar fraction, T_0 represents the reference environment temperature (298.15 °C), R shows the gas constant ($R = \frac{8.314}{M_G}$), and G^E describes Gibbs' free energy.

The exergy destruction calculation method in RO and the chemical exergy of seawater are investigated in Sharqawy et al. (2011).

Table 6
The molar fraction and chemical exergy of reforming products (Sharqawy et al., 2011).

Component	Molar fraction (%)	Chemical exergy (kJ/kmol)
CO	Negligible	269412
CO_2	16.04	14176
H_2	Negligible	235249
H_2O	21.99	8636
N_2	60.49	639
O_2	1.48	3951

By differentiating the total Gibbs energy function concerning the composition, the chemical potentials of water and salts in seawater are calculated as follows (Sharqawy et al., 2011):

$$\mu_w = \frac{\partial G_{sw}}{\partial m_w} = g_w - w_s \frac{\partial g_{sw}}{\partial w_w} \quad (15)$$

where w and μ, and are respectively mass fraction and chemical potential, g_{sw} presents the specific Gibbs seawater energy determined below.

$$g_{sw} = h_{sw} - (T - 273.15) s_{sw} \quad (16)$$

The entropy and enthalpy correlations can be used for calculating the specific Gibbs energy function by Mokhtari et al. (2016b). Using the entropy and enthalpy correlations, the specific Gibbs energy differentiation with respect to salt concentration is conducted as below (Sharqawy et al., 2011):

$$\frac{\partial g_{sw}}{\partial s_s} = \frac{\partial h_{sw}}{\partial s_s} - (T - 273.15) \frac{\partial s}{\partial s_s} \quad (17)$$

The chemical exergy of salty water is calculated as (18). The entropy and enthalpy differentiation with respect to the salt concentration is achieved based on (Khanarmuei et al., 2017; Sharqawy et al., 2011):

$$ex_{sw}^{ch} = \sum_{i=1}^{n} w_i (\mu_i - \mu_0) \quad (18)$$

Ultimately, exergy destruction ($\dot{Ex}_D$) is calculated by (19) (Bejan and Moran, 1996; Mokhtari et al., 2017):

$$\dot{Ex}_Q + \sum_i \dot{m}_i ex_i = \sum_e \dot{m}_e ex_e + \dot{Ex}_W + \dot{Ex}_D \quad (19)$$

$\dot{Ex}_W$ and $\dot{Ex}_Q$ are the exergy related to work and heat transfer. Which $\dot{Ex}_D$ shows exergy destruction and ex presents the amount of specific exergy (Bejan and Moran, 1996; Mokhtari et al., 2017):

$$\dot{Ex}_D = T_0 \dot{S}_{gen} \quad (20)$$

$$\dot{Ex}_Q = \int_i^e \left(1 - \frac{T_0}{T_w} \right) q' \, dL \quad (21)$$

$$\dot{Ex}_W = \dot{W} - p_0 \frac{dV_{cv}}{dt} \quad (22)$$

$\dot{Ex}_w$ shows work exergy rate. Indices 0, e i and are respectively ambient environment, output, and input. It is worthy to note that T in relations (21) and (22) should be in Kelvin unit.

As a result, the exact amount of exergy destruction can be calculated as below (Bejan and Moran, 1996; Mokhtari et al., 2017):

$$\dot{Ex}_f = \dot{Ex}_P + \dot{Ex}_D + \dot{Ex}_L \quad (23)$$

In Eq. (23), $\dot{Ex}_f$, $\dot{Ex}_P$, $\dot{Ex}_L$ are fuel exergy, exergy product, and exergy loss, respectively.

The ratio of exergy destruction rate to the total exergy destruction rate could be obtained by introducing the following parameter (Bejan and Moran, 1996):

$$y_D = \frac{\dot{Ex}_D}{\dot{Ex}_{D,Total}} \tag{24}$$

The cycle exergy efficiency is computed as below (Bejan and Moran, 1996):

$$\eta_{ex} = \frac{\dot{Ex}_p}{\dot{Ex}_{f,int,Plant}} \xrightarrow{Eq(23)}$$
$$= 1 - \frac{\dot{Ex}_D + \dot{Ex}_L}{\dot{Ex}_{f,int,Plant}} \tag{25}$$

where $\dot{Ex}_{f,int,Plant}$ shows the inlet exergy from combustion products.

4.3. Economic analysis (3E)

In addition to technical study and thermodynamic restrictions, an economic analysis is necessary for determining and selecting a plan. Typically, TAC consists of two terms, total capacity investment (TCI) and operating costs (OC). TCI consists of the total cost of fixed capital investment (FCI), startup costs (SUC) and working costs (WC), research and development costs (R&D), licensing cost, and allowance for funds used during construction (AFUDC) Eq. (26) (Bejan and Moran, 1996).

$$TCI = FCI + SUC + WC + LRD + AFUDC \tag{26}$$

Eq. (27) is used for calculating direct project costs (DC), which consists of off-site cost (OFSC) and on-site cost (ONSC) (Bejan and Moran, 1996):

$$DC = ONSC + OFSC \tag{27}$$

The FCI costs include indirect cost (IC) and DC cost. According to the estimations, the IC cost is equal to 25% of DC cost (Bejan and Moran, 1996):

$$FCI = 1.25\,DC \tag{28}$$

The OFSC for an expansion of an existing facility could be 40% to 50% (average value 45%) of the ONSC or the OFSC for the construction of a new facility is between 100% to 200% (average value 120%) of ONSC (Mokhtari et al., 2016a):

$$OFSC = \begin{cases} 1.2 \times ONSC & new\ system \\ 0.45 \times ONSC & expansion \end{cases} \tag{29}$$

According to the overall approximation, the SUC and WC are respectively 10% and 15% of TCI (Bejan and Moran, 1996):

$$SUC = 0.10\,FCI \tag{30}$$

$$WC = 0.15 \times TCI \tag{31}$$

R&D cost is assumed to obtain by the following equation (Bejan and Moran, 1996):

$$AFUDC + LRD = 0.15\,FCI \tag{32}$$

That is to say, the sum of AFUDC and LRD would be 15% of FCI cost (Mokhtari et al., 2016a). Based on FCI and according to (26), (30), (31), (32), TCI is introduced as follows.

$$TCI = 1.47\,FCI \tag{33}$$

The coefficient 1.47 is achieved according to the above-mentioned simple algebraic equations demonstrating that TCI

cost is equal to 147% of FCI cost. It is possible to define TCI according to FCI price anticipation in relation (28) in the form of DC or (ONSC + OFSC) (Bejan and Moran, 1996):

$$TCI = 1.84\,DC = 1.84\,(ONSC + OFSC) \tag{34}$$

By replacing 184% from (34) in (29), TCI is described according to each novel or expansion system (Bejan and Moran, 1996):

$$TCI = \begin{cases} 4.05 \times ONSC & new\ system \\ 2.67 \times ONSC & expansion \end{cases} \tag{35}$$

For a new system, the FCI is typically in the range of 280% to 550% of capital cost (CC) with an average value of 430% (Mokhtari et al., 2016a). The FCI average is around 283% of CC for an expansion system (Mokhtari et al., 2016a):

$$FCI = \begin{cases} 4.30\ CC & (new\ system) \\ 2.83\ CC & (expansion) \end{cases} \tag{36}$$

Based on (33), the cost of TCI is presented as a percentage of CC in the form of (37) (Mokhtari et al., 2016a):

$$TCI = \begin{cases} 6.32\ CC & (new\ system) \\ 4.16\ CC & (expansion) \end{cases} \tag{37}$$

TCI costs can be normalized and divided into annual operating cost and useful longevity cost. The value of TAC is obtained as follows (Mokhtari et al., 2016a):

$$TAC = AOC + TCI/CRF \tag{38}$$

CRF represents cost recovery factor which is dependent on the approximate lifetime of the components and Interest Rate (IR), which can be calculated by (39) (Bejan and Moran, 1996; Ameri et al., 2016):

$$CRF = \frac{i(1 + i)^{yr}}{i(1 + i)^{yr} - 1} \tag{39}$$

where i and yr are respectively IR ($=10\%$) and effective lifetime ($=20$ years) of the project (Dai et al., 2009).

For each component, the AOC is considered 2% of CC, as mentioned in Bejan and Moran (1996).

The CC of RO is obtained from reference (Mokhtari et al., 2016a) relations. These relations are divided into the costs of membrane replacement and the annual operation cost, including Laboratory, Insurance, and Additive Chemicals (Birnhack et al., 2011; Macchi and Astolfi, 2016).

4.4. Environmental effect (4E)

- Power generation section

In this paper, the fluids are chosen among 58 organic fluids (Bao et al., 2018a; ANSI/ASHRAE Standard 34-2007, 2007). They belong to cycloalkanes, Aliene and alkynes, Alcohols, and ketones, and Refrigerant fluids siloxanes are obtained based on the following process. The working fluid selection is initially according to the flammability. Therefore, fluids with high flammability are not considered. Then the fluids that their critical temperature is far from the temperature of heat resource are omitted. The fluids with the critical temperature range close to the heat resource increase the efficiency of the system, based on the literature review. Ultimately, the optimum selection of the organic fluid with the configuration of the ORC in terms of the 4E concept is made by the GA, similar to what is done in references Mokhtari et al. (2016a), Bao et al. (2018b) and Voutchkov (2011).

The organic fluids contain two indices for the rate of environmental impacts, which are ODP and GWP.

Table 7

The thermodynamic parameters and environmental fluids indices (Henthorne and Boysen, 2015).

No.	fluid	$P_{critical}$ (MPa)	$T_{critical}$ (°C)	ODP	GWP	ASHRAE Standard 34[a]
1	R141b	4.212	204.4	0.11	700	–
2	R11	4.408	198	1	4750	A1
3	R364mfc	3.271	186.9	–	890	–
4	R123	3.662	183.7	0.02	120	B1
5	R245ca	3.925	174.4	0	640	–
6	R1233zd	3.6237	166.45	0.00034	4.5	A1
7	R245fa	3.651	154	0	950	B1
8	R114	3.289	146	1	10040	A1
9	R236ea	3.502	139.3	0	1200	–
10	R236fa	3.2	125.7	0	1030	B1

[a]Refrigerant safety group classification. 1: No flame propagation; 2: Lower flammability; 3: Higher flammability; A: Lower toxicity; B: Higher.

Table 7 illustrates the pressure and critical temperature, the ODP, and GWP rate with a safety factor of each of the working fluids. The lowest environment destruction index belongs to the R1233zd, among other fluids. After R1233zd, the R123 and R245ca are the other fluids with the minimum index. The items that are important to choose the fluid are as follows:

– low ODP and GWP
– not being toxic
– low flammability
– having the minimum cost of insulation
– higher condenser pressure compared to ambient pressure to decrease the accessories cost.

Also, the items mentioned in references Mokhtari et al. (2016a), Sharqawy et al. (2011) and Henthorne and Boysen (2015) are the decision factors for organic fluid.

● *The RO section*

In this section, the environmental effects are (1) the brine (concentrate disposal) of RO outlet water and (2) the additive chemicals for pre-refinement of RO (Doneker and Jirka, 2001; Loya-Fernández et al., 2012).

The focus of this paper is to produce more permeate water and reduce the environmental effects of brine discharge to sea by raising the temperature of the feed flow to RO (See Section 3).

Considering the buoyancy force, which depends on the density difference, the non-dimensional function Ω is defined in this section. The denominator of this function is the density difference of seawater with the density of the waste with no preheat (stream 15), and the numerator is the density difference with preheating.

$$\Omega = \frac{(\rho_{15} - \rho_{sw})_{\text{Preheating}}}{(\rho_{15} - \rho_{sw})_{\text{Without preheating}}} \quad (40)$$

For a better understanding of this concept, this amount is shown in percent $\bar{\Omega} = 100 \times (1 - \Omega)$.

5. Optimization

In order to optimize a thermodynamic system, the objective function, the optimization characteristics, and the decision parameters are needed for GA. The decision parameters in this paper are introduced according to Table 8. For determining the

membranes and configuration, an integer is designated for each of the parameters. When the GA chooses this integer, the desired cycle or fluid are selected and analyzed.

The optimization process is shown in Fig. 5. Different organic fluids are filtered based on the case study conditions before optimization, and ultimately ten working fluids are selected. Some optimization parameters and the factors that affect the objective function are shown in this figure.

The influential factors in selecting organic fluid are the proximity of the critical temperature to the temperature of the heat source, non-flammability, and non-toxicity. At first, organic fluids are selected accordingly. The final fluid is selected based on the environmental impact filter. These fluids can be placed as variables in different cycles and participate in optimization as a decision parameter. On the other hand, other thermodynamic parameters of the membrane type affect the selected target functions of energy and exergy efficiencies, environmental impacts, and water cost. The GA determines the optimal value of these parameters.

The ultimate price of freshwater/unit product cost (UPC) and the exergy efficiency should be considered for determining the objective function. The price of freshwater is calculated by Eq. (41):

$$Cost_{water} = \frac{TAC_{RO} + TAC_{ORC}}{\dot{Q}_p \times 365 \times 24 \times f_c} \quad (41)$$

This equation represents that the ultimate price of freshwater/UPC is the sum of TAC of the ORC and RO side. This price is calculated according to fresh water and the system performance coefficient (f_c) of 0.9 from reference Mokhtari et al. (2016a). The exergy efficiency is obtained from Eq. (25). In this paper, an optimization code is developed and solved in MATLAB software. The mutation and crossover probabilities are respectively set to 5% and 90% [117,117].

Regarding the outputs of the GA in multi-objective optimization, the best point in Pareto curve is determined according to the reference Sayyaadi and Mehrabipour (2012), and the results are shown based on that.

6. Validation

The cycle contains two parts; hence, this study is introduced in two parts too.

● *The ORC section*

Table 8
The decision parameters with upper and lower limits.

Parameters	Unit	Up boundary	Low boundary	Explanations
Approach temperature (Mokhtari et al., 2016a; Llor, 2005)	°C	5	10	–
Configuration type (Nabati et al., 2018; Beni et al., 2021)	–	1	4	1: Cycle A; 2: Cycle B; 3: Cycle C; 4: Cycle D
Condenser temperature (Shayesteh et al., 2019; Ameri et al., 2018)	°C	40	60	The temperature of Persian gulf water increase to 35 °C
Heat exchanger pressure in cycle C and D	kPa	4000	800	–
Inlet and outlet water difference (Safarian and Aramoun, 2015)	°C	5	10	Economic issues and tubes expansion and contraction
Pinch temperature (Mokhtari et al., 2017)	°C	10	150	–
Number of stages (Khanarmuei et al., 2017)	–	1	2	–
Number of membranes in each PV (Mokhtari et al., 2016d)	–	2	8	According to DOW recommendation
Recovery (Khanarmuei et al., 2017; Mokhtari et al., 2016d)	%	10	55	According to DOW recommendation
Turbine inlet pressure (Ameri et al., 2016)	kPa	4200	700	–
The type of membrane in second stage (Shayesteh et al., 2019)	–	1	23	The type of BW and SW membranes of DOW[a]
The type of membrane in first stage (Shayesteh et al., 2019)	–	1	9	The type of membrane from DOW[a] company
The rejected water percentage (Shayesteh et al., 2019)	%	0	95	–
Working fluid type (Shayesteh et al., 2019)	–	1	10	[b]

[a]The allocated numbers indicate: 1: SW30XLE-400i; 2: SW30HR-320; 3: SW30HRLE-370 34i, 4:SW30ULE-440i; 5: SW30HR LE-400; 5: SW30HR LE-400i; 7: SW30ULE-400i 8: SW30ULE-440i2 9: SW30XLE-440i; 10: BW30-365; 11: BW30FR-365; 12: BW30-400 13: BW30FR-400; 14: BW30-400i; 15: BW30-400-34; 16: BW30-400-34i; 17: BW30XFR-400-34; 18: BW30XFR-400-34i; 19: BW30XFRLE-400-34; 20: BW30XFRLE-400-34i; 21: BW30HR-440i; 22: BW30HRLE-440; 23: BW30HRLE-440i.
[b]The allocated code to each fluid is according to Table 6 rows.

Table 9
The validation results of this study compared with Ref. Safarian and Aramoun (2015).

Parameter	Unit	Present study	Safarian and Aramoun (2015)
Condenser duty	kW	196.0	194.6
Evaporator duty	kW	252	252
Net power	kW	57.94	57.54
Pump power	kW	4.06	3.46
Thermal efficiency	%	22.99	22.83
Turbine power	kW	62	61
Mass flow (organic fluid)	kg/s	1.96	1.91

The organic fluid properties are derived from REFPROP software (Bao et al., 2018a). The validation of the ORC side is done for each cycle comparing with the reference (Safarian and Aramoun, 2015). The results of cycle D are presented in this paper, and the results of other cycles are not shown to summarize the paper. As one can see, the errors in this section are acceptable (Table 9).

● *The RO section*

Companies develop software according to the membranes it produces, and the data of these membranes are saved to the database of the company. In this section, DOW software with the commercial name of ROSA name is used for validating the developed MATLAB code. The code used in this paper is the code for references Mokhtari et al. (2016a), Khanarmuei et al. (2017) and Mokhtari et al. (2016d), and so the validation results are mentioned in reference Mokhtari et al. (2016a).
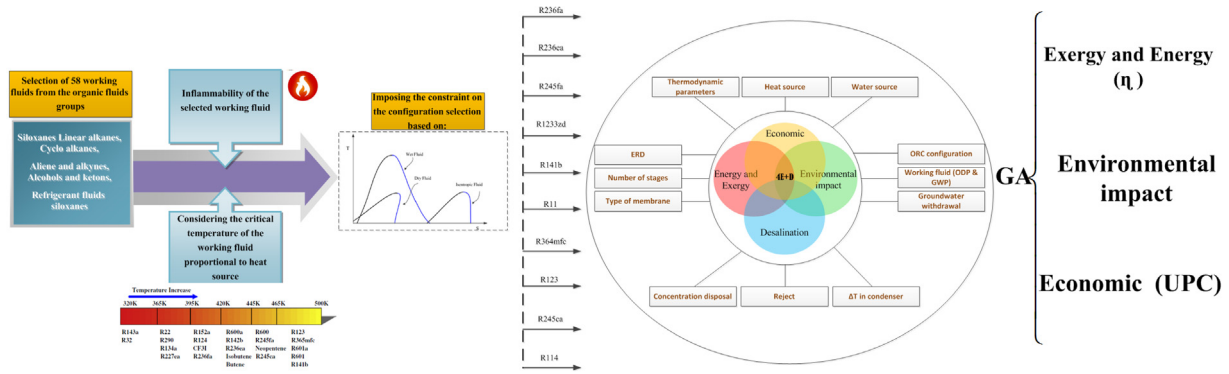
Fig. 5. Flowchart of working fluids determination and ultimate selection of them by the GA.
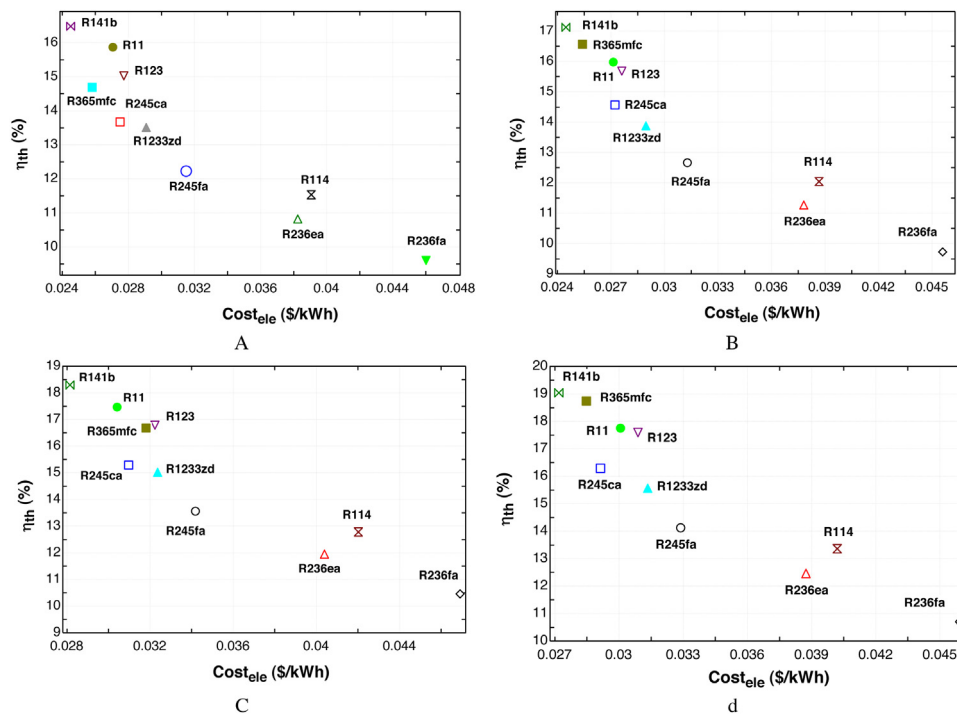

Fig. 6. Evaluation of the price for electricity produced for different fluids. (a) cycle A, (b) cycle B, (c) cycle C, (d) cycle D.

7. Results

According to this fact, that the system consists of two major sectors, the ORC and the RO+ERD, the results are expressed based on these two parts, and the GA is used for optimizing the net system based on decision parameters. Two main parameters for each power cycle in the thermo-economic analysis are thermal efficiency and the price of produced electricity. Fig. 6 shows the results of investigating these two parameters among case study cycles with different fluids.

According to Table 7, the results clearly demonstrate that fluids with higher critical temperatures have more suitable thermal efficiencies. The higher net power production causes an increase in cycle efficiency for constant pinch and approach temperatures. In Fig. 6, the results are specifically due to the type of working fluid, and other parameters considered constant in this study. The net price for electricity production is related to two parameters of TAC and W_{net}. In this study, it is observed that the efficiency differs just a little for fluids like R364mfc and R123 in each configuration.

The other important point in this figure is the change in efficiency with configuration. The thermal efficiency increases with moving from Cycle A to Cycle D. Ultimately, the fluids in cycle D have maximum thermal efficiency.

The study of the second law of thermodynamics for different cycles reveals that Cycle A has the maximum exergy efficiency among other cycles (Fig. 7). By considering the pinch and approach temperature, the rate of energy recovery in WHR to be constant by moving from Cycle A to Cycle D, the fuel exergy and system production is reduced, and exergy loss increases. As a result, the exergy efficiency in the simple cycle is more than in other cycles.

Among different fluids, the R236fa and R245ea have the highest exergy efficiency. The exergy loss is due to an increase in WHR stack exhaust gases, and this exergy flow is called exergy loss since it is not useful because of the acid dew point limit. From another perspective, in order to avoid the economizer tube corrosion, the system does not use this exergy. It is possible to minimize these losses by changing the design and pinch temperature.

In exergy analysis, it can be stated for fluid R245fa that in Cycles A, B, C, and D, the total amount of total exergy degradation is 282, 344, 353, and 390 kW, respectively. It is observed that
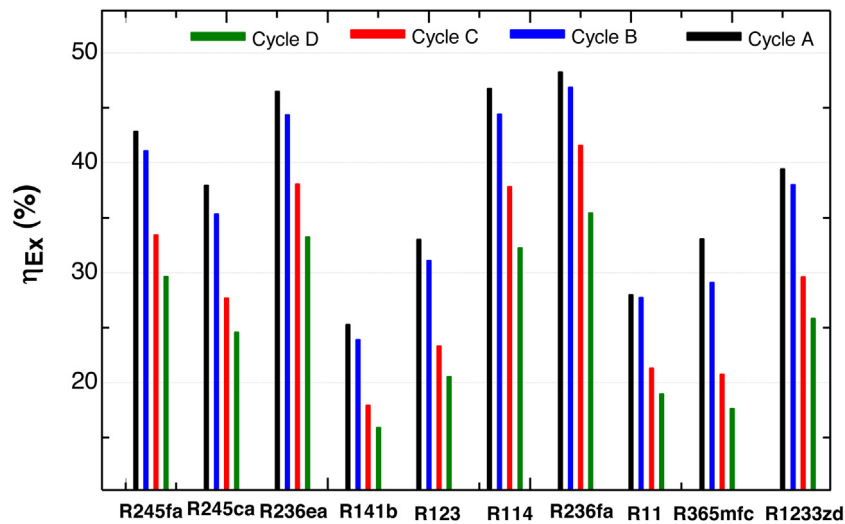
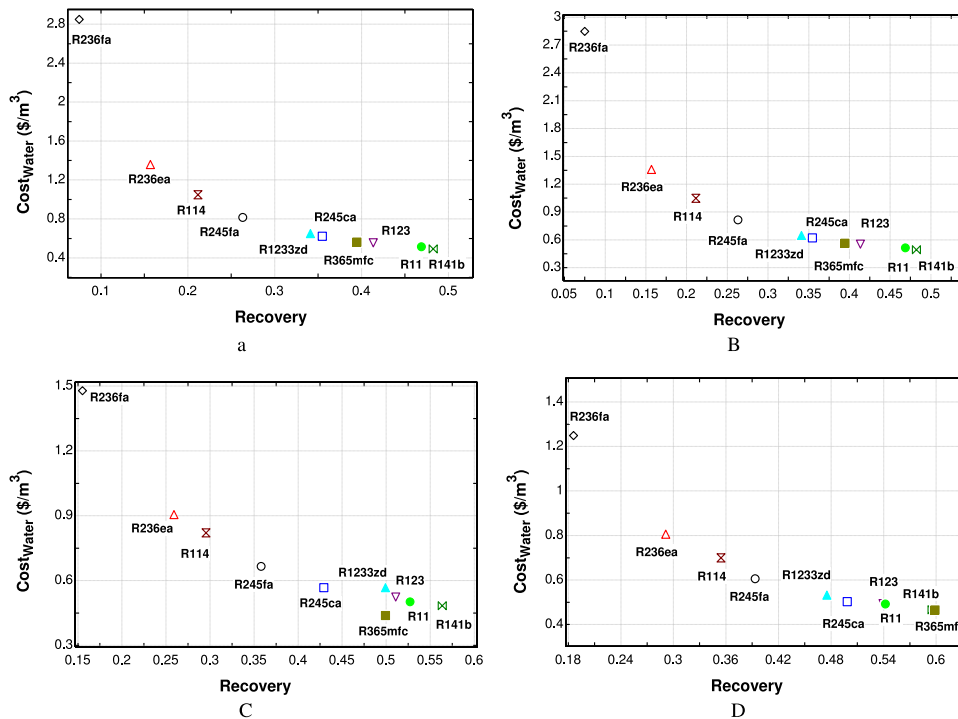**Fig. 7.** The exergy efficiency of case study cycles with different fluids.

Fig. 8. The price of produced water among different fluids (a) cycle A, (b) cycle B, (c) cycle C, (d) cycle.

Table 10
Exergy degradation rate between equipment in different cycles.

	HRSG	Turbine	Condenser	Pump 1	Pump 2	OFOH	HEX	Total (kW)
Cycle A	161.64	82.37	22.20	15.95	0.00	0.00	0.00	282.16
Cycle B	166.87	82.37	24.02	15.95	0.00	0.00	55.03	344.25
Cycle C	177.81	82.58	22.20	16.03	29.72	25.00	0.00	353.34
Cycle D	177.81	82.52	24.12	16.03	29.99	39.03	20.60	390.10

with increasing exergy degradation, the total exergy efficiency decreases. External degradation of each piece of equipment can be seen in Table 10. Among the equipment, due to the temperature difference between hot and cold currents, the amount of exergy degradation in HRSG is more than the equipment delay.

Fig. 8 represents the UPC and RO system recovery. There are some parameters that are directly effective in the determination of these two parameters. The fluid rejection, net power, and the RO system number of stages are some examples. The temperature difference is constant in various modes, so the heat transferred
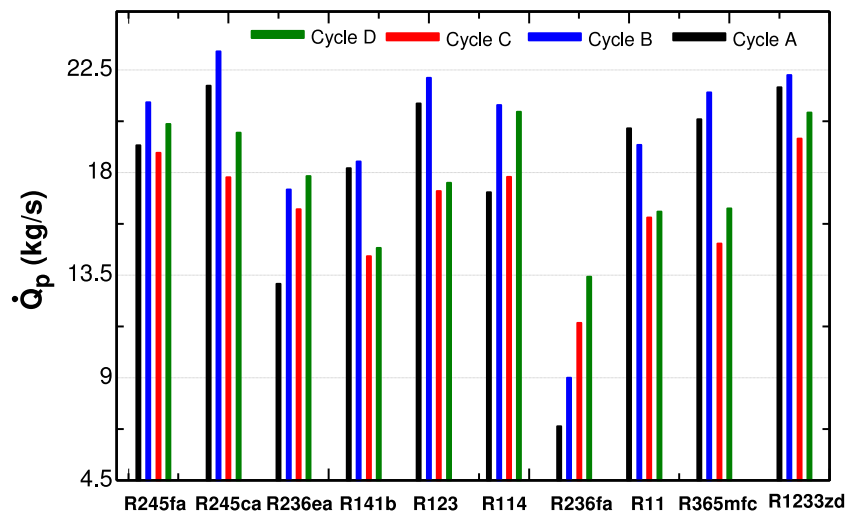
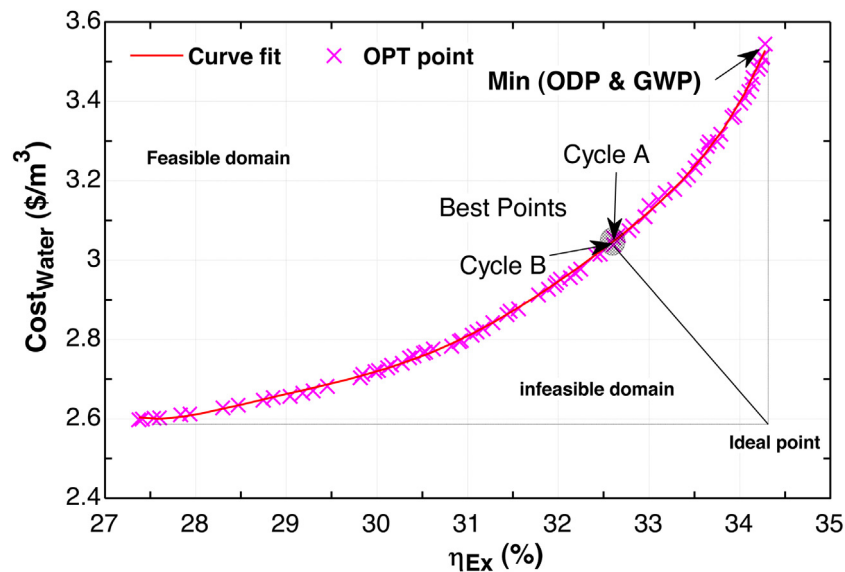**Fig. 9.** The produced water in different cycles with various fluids.

Fig. 10. The Pareto curve from multi-objective optimization.

to the cooling water of the condenser in cycle A is more than in other configurations.

- This causes an increase in the feed flow rate of RO. Therefore, the net power produced is utilized for the RO pump; the generated pressure is inversely proportional to the feed flow rate based on the pump power relations. If the flow rate increases, the feed pressure decreases.

According to relation (1), by reducing the difference between feed pressure and osmosis pressure $(P_f - \pi)$, the amount of J_W reduces. In this condition, the freshwater flow rate decreases, which means that the number of membranes in each PV should be increased for obtaining more freshwater. Also, by the constant membranes, the number of stages in RO increases. For both of these two modes, the costs increase. The only factor which is able to change the feed pressure in a configuration is changing the working fluid, and this procedure is presented in Fig. 8.

The cycle with R141b produces more freshwater with a lower net price due to higher power. In other configurations, by reducing the absorbed heat in the condenser, the water flow rate reduces at a constant temperature, which affects the feed pressure and increases the freshwater flow.

The other factors, like TCF, mentioned in (9) also increase the freshwater flow rate. This factor impacts the freshwater quality. The difference between the inlet/outlet water temperature in the condenser is constant and equal to 10 °C.

The recovery factor is obtained from feed water flow and freshwater. According to Fig. 9, the R245ca working fluid has the highest freshwater production, but the recovery factor for this fluid is lower than some others. The reason is the heat transfer in the condenser section and entrance of feed water to RO. For improving recovery factor, there are a number of ways like the type of configuration, membranes, and the design of RO.

As shown in analysis and investigations, the aforementioned system should be analyzed in terms of 4E and an integrated system for choosing the optimal parameters. The interaction between the ORC and RO parameters impacts the system's ultimate goal, which is the exergy efficiency and the net price of water. Fig. 10 presents the results of optimization by utilizing the GA and decision parameters.

The optimization result is the Pareto curve which divides the results into two feasible and infeasible domains. The ideal point is obtained by the cross-section of two tangent lines on the Pareto curve. This ideal point has the least price of water and the

Table 11
The main parameters of the two chosen optimum cycles.

| Parameter	Symbol	Best point (1)	Best point (2)	Min (OPD & GWP)
ORC configuration		Cycle A	Cycle B	Cycle B
Total annual cost ($/year)	TAC	461093.5	448662.41	626286.0
ORC exergy efficiency (%)	$\eta_{Ex,ORC}$	31.27	28.74	19.6
Total exergy efficiency (%)	η_{Ex}	32.51	32.49	34.18
Net power plant (MW)	$\dot{W}_{net}$	1.388	1.389	1.02
Energy efficiency ORC (%)	η_{Th}	11.27	11.79	13.9
Water product (m³/h)	$\dot{Q}_p$	266.65	278.53	201.96
The feed pressure (bars)	P_f	63.1	72.0	62.8
Concentration of permeate (ppm)	C_p	831.36	756.36	245.88
Specific energy consumption (kWh/m³)	SEC	2.31	2.55	2.49
Recovery (%)	R	39.24	46.82	28.46
Total exergy destruction (MW)	$\dot{Ex}_D$	3.19	3.31	2.96
Unit product cost ($/m³)	$Cost_{water}$	2.84	2.64	3.54
Outlet Temp blast furnace combustion products (°C)	$T_{gas,o,eco}$	132	141	156.7
Type of membrane	–	SW30XLE-400i	SW30XLE-400i	SW30HRLE-370 34i
Number of stage	–	1	1	1
Energy recovery device	ERD	Turbine	Turbine	Turbine
Energy recovery (kW)	–	691.95	597.0	584.0
$\overline{\Omega}(\%)$	–	16.94	12.74	26.52
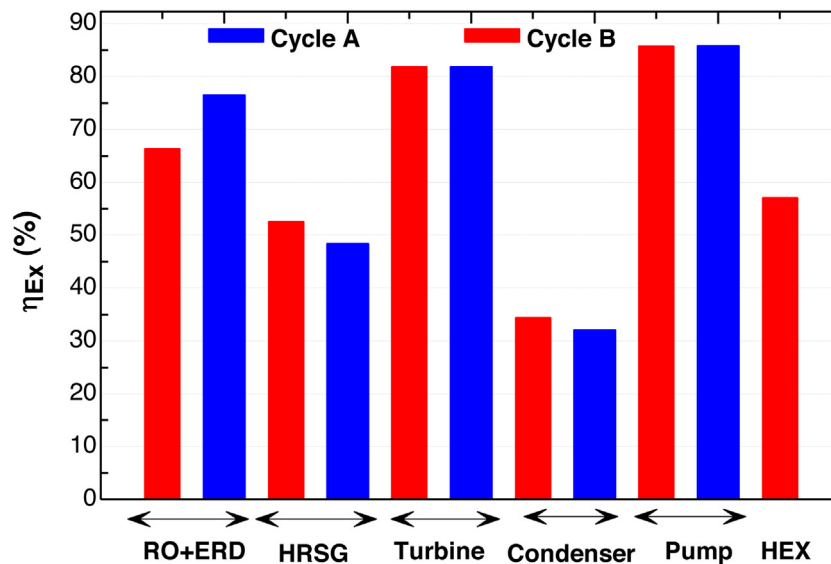
Fig. 11. The comparison of exergy efficiency for each component in two optimum cycles of A and B.

highest exergy efficiency in the infeasible domain. Each point of the Pareto curve, which is closer to the ideal point, is the best point of curve points collection.

According to the fresh water and exergy efficiency of the whole system, each point can be chosen and studied, and the best points are chosen based on the procedure introduced in Fig. 10. According to this procedure, Cycles A and B are chosen as the two optimal cycles. The important parameters from optimized points are shown in Table 11. By fitting a curve on the points,

the equation is obtained, which is shown as follows. This equation provides the direct relation between the exergy efficiency and the UPC.

$$Cost_{water} = 118682 - 23390.3 \cdot \eta_{Ex} + 1918.78 \cdot \eta_{Ex}^2 - 83.8596 \cdot \eta_{Ex}^3 + 2.05944 \cdot \eta_{Ex}^4 - 0.0269461 \cdot \eta_{Ex}^5 + 0.000146756 \cdot \eta_{Ex}^6$$

It can be concluded from Table 11 that the whole system's exergy efficiency in Cycle A is greater than other cycles, and

Table 12
The results of energy and exergy analysis of cycle A in optimum mode.

Point	Substance	Mass flow rate (kg/s)	Temperature (K)	Pressure (bars)	$\dot{Ex}$ (kw)	Component
1	R245ca	49.89	313.73	1.76	30.67	$CHF_2CF_2CH_2F$
2	R245ca	49.89	314.11	11.046	65.31	$CHF_2CF_2CH_2F$
3	R245ca	49.89	380.76	11.046	2367.2	$CHF_2CF_2CH_2F$
4	R245ca	49.89	337.92	1.76	619.63	$CHF_2CF_2CH_2F$
5	Blast furnace combustion products	75	545	0.995	4605.3	N_2:60.49% ; O_2:1.48% ; CO_2: 16.04%; H_2O:21.99%
6	Blast furnace combustion products	75	405	1.0	98.23	N_2:60.49% ; O_2:1.48% ; CO_2: 16.04%; H_2O:21.99%
7	Seawater	261.97	298	2.0	0.0	TDS = 46000 ppm, SDI = 5<
8	Seawater	261.97	307.98	2.0	188.0	TDS = 46000 ppm, SDI = 5<
9	Seawater	188.75	307.98	2.0	135.4	TDS = 46000 ppm, SDI = 5<
10	Seawater	73.22	307.98	2.0	52.55	TDS = 46000 ppm, SDI = 5<
11	Seawater	188.75	307.98	63.1	135.4 /0.0[a]	TDS = 46000 ppm, SDI = 2<
12	Water/Brian	114.68	307.98	62.78	580.2	TDS = 75175 ppm
13	Water/Permeate	74.07	307.98	1.0	-47.76	TDS = 831.36 ppm

[a]Based on reference Sharqawy et al. (2011).

Table 13
The results of energy and exergy analysis of cycle B in optimum mode.

Point	Substance	Mass flow rate (kg/s)	Temperature (K)	Pressure (bars)	$\dot{Ex}$ (kw)	Component
1	R245ca	49.92	313.72	1.76	30.67	$CHF_2CF_2CH_2F$
2	R245ca	49.92	314.11	11.046	65.4	$CHF_2CF_2CH_2F$
3	R245ca	49.92	324.88	11.046	96.6	$CHF_2CF_2CH_2F$
4	R245ca	49.92	380.75	11.046	2369.1	$CHF_2CF_2CH_2F$
5	R245ca	49.92	337.91	1.76	619.63	$CHF_2CF_2CH_2F$
6	R245ca	49.92	318.56	1.76	532.7	$CHF_2CF_2CH_2F$
7	Blast furnace combustion products	75	545	0.995	4605.3	N_2:60.49% ; O_2:1.48% ; CO_2: 16.04%; H_2O:21.99%
8	Blast furnace combustion products	75	414.11	1.0	112.47	N_2:60.49% ; O_2:1.48% ; CO_2: 16.04%; H_2O:21.99%
9	Seawater	238.96	298	1.0	0.0	TDS = 46000 ppm, SDI = 5<
10	Seawater	238.96	307.99	2.0	172.4	TDS = 46000 ppm, SDI = 5<
11	Seawater	165.22	307.99	2.0	119.2	TDS = 46000 ppm, SDI = 5<
12	Seawater	73.74	307.99	2.0	53.2	TDS = 46000 ppm, SDI = 5<
13	Seawater	165.22	307.99	72.08	119.2 /0.0[a]	TDS = 46000 ppm, SDI = 2<
14	Water/Brian	87.85	307.99	71.72	581.26	TDS = 85846 ppm
15	Water/Permeate	77.37	307.98	1.0	-56.10	TDS = 756.34 ppm

[a]Based on reference Sharqawy et al. (2011).

Table 14
The selection of the optimum point from the Pareto curve based on considering the minimum organic fluid environmental impacts.

Point	Substance	Mass flow rate (kg/s)	Temperature (K)	Pressure (bars)	$E\dot{x}$ (kW)	Component
1	R1233zd	47.19	319.74	2.64	50.37	$C_3H_2ClF_3$
2	R1233zd	47.19	320.91	23.35	131.7	$C_3H_2ClF_3$
3	R1233zd	47.19	329.60	23.35	121.9	$C_3H_2ClF_3$
4	R1233zd	47.19	414.18	23.35	2582.1	$C_3H_2ClF_3$
5	R1233zd	47.19	339.8	2.64	703.6	$C_3H_2ClF_3$
6	R1233zd	47.19	323.51	2.64	638.4	$C_3H_2ClF_3$
7	Blast furnace combustion products	75	545	0.995	4605.3	N_2:60.49% ; O_2:1.48% ; CO_2: 16.04%; H_2O:21.99%
8	Blast furnace combustion products	75	429.74	1.0	169.7	N_2:60.49%; O_2:1.48%; CO_2: 16.04%; H_2O:21.99%
9	Seawater	284.13	298	1.0	0.0	TDS = 46000 ppm, SDI = 5<
10	Seawater	284.13	307.99	2.0	169.7	TDS = 46000 ppm, SDI = 5<
11	Seawater	284.13	307.99	2.0	169.7	TDS = 46000 ppm, SDI = 5<
12	Seawater	140.18	307.99	2.0	108.5	TDS = 46000 ppm, SDI = 5<
13	Seawater	143.95	307.99	62.81	109.2 /0.0[a]	TDS = 46000 ppm, SDI = 2<
14	Water/Brian	87.85	307.99	62.20	363.6	TDS = 64200 ppm
15	Water/Permeate	56.10	307.98	1.0	−36.10	TDS = 245.88 ppm

[a]Based on reference Sharqawy et al. (2011).

the net price of produced electricity is lower in Cycle B. Fig. 11 represents the exergy efficiency of each equipment in Cycles A and B. The results demonstrate that the RO has the SEC of 5.17 kWh/m³ and the exergy destruction and efficiency of 856 KW and 38.33 percent, respectively. By utilizing the ERD system indicated in Table 11, all the parameters like SEC, the exergy destruction, exergy efficiency are 2.31 kWh/m³, 76.4%, and 164.41 kW, respectively. The recovered power in the ERD system is also demonstrated in Table 11. The WHR has more entropy generation. The exergy destruction compared with other equipment and the reason is the difference between the cold and hot streams. This exergy destruction allocates 75% of the exergy destruction of the whole system. In Tables 12 and 13, the results of exergy and energy analyses for each point of the cycle are shown. The silt density index (SDI) is the water quality index.

Table 14 is introduced among the Pareto points based on Min (ODP&GWP) and environmental impacts. Cycle B is selected with the working fluid R123zd by the GA. The cycle exergy efficiency equals 34.28%, and the net price is 3.54 $/m³. The organic fluid has the minimum environmental impact at this point. Still, the amount of water production decreases. This point has more water withdrawal from groundwater than the best points. Despite this fact, the amount of Ω improves and causes a 26.5 percent decline in dilution span.

8. Conclusions

The studies indicate that configuration and working fluid selection for ORC is dependent on important parameters like (1) the ultimate goal of cogeneration and utilizing ORC. (2) The conditions of low pressure and high-pressure thermal sources. (3) The governing constraints on the recovery system. These

parameters should be considered in each analysis. In this paper, cogeneration and utilizing ORC produce water for the steel process and raise system efficiency. The acid dew point is one of the constraints on the organic Rankine cycle. Based on exhaust gases of steel enterprise furnaces, one practical approach for reducing the environmental impacts of RO system concentrate disposal is preheating the water coming to the RO system. By utilizing this approach, the interaction between RO and ORC increases. The reason is that the condenser affects RO performance. By determining optimum parameters related to the case study system, the GA demonstrated that the basic ORC with R245ca and the one stage RO system with SW30XLE-400i membrane could reach the overall exergy efficiency of 34.81% and the net price of 2.84 $/m³ for water. For optimum ORC points with recuperator and the working fluid of R245ca and the one stage RO system with SW30XLE-400i membrane, the net exergy efficiency of the system and the ultimate price of water/UPC are 34.49% and 2.64 $/m³, respectively.

Nomenclature

Subscripts

A	Area (m²)
A_w	Coefficient of water permeability (kg/m² s Pa)
AFUDC	Allowance for Funds Used During Construction ($)
AOC	Annual Operating Cost ($/year)
B	Coefficient of solute transport (kg/m² s)

C	Concentration (ppm)
C_f	Feed-water concentration (ppm)
C_b	Brine concentration (ppm)
C_p	Permeate concentration (ppm)
Cp	Specific heat at constant pressure (kJ/kg K)
CC	Purchasing cost/capital cost ($)
CRF	Cost recovery factor
DC	Direct costs ($)
$\dot{Ex}$	Exergy rare (kW)
ex	Specific exergy (kJ/kg)
FF	Fouling factor
f_c	System performance coefficient
FCI	Fixed capital investment ($)
h	Enthalpy (kJ/kg)
i	Interest rate
IC	Indirect cost ($)
J_w	Local permeate flux (kg/m^2 s)
J_s	Local solute flux (kg/m^2 s)
K	Local mass transfer coefficient (m/s)
LRD	Licensing, Research and Development Costs ($)
$\dot{m}$	Mass flow rate (kg/s)
OFSC	Off-site cost ($)
ONSC	On-site cost ($)
P	Pressure (bar or kPa)
pf$_i$	Modified density polarization
P_f	Feed-water pressure (bar)
$\dot{Q}$	Heat (kW) / Flow rate (m^3/h)
R	Gas constant (kJ/kg K)/ Recovery (%)
R_e	Reynolds number
S	Entropy (kJ/kg)
SR	Salt rejection (%)
S_m	Membrane area (m^2)
SUC	Start-up costs ($)
T	Temperature (°C)
TAC	Total annual cost ($/year)
TCI	Total capacity investment ($)
U	Overall heat transfer coefficient (W/m^2 ° C)
V_w	Permeate velocity (m/s)
$\dot{W}$	Work rate (kW)
W	Work (kJ/kg)
WC	Working costs ($)
w_g	Mass fraction
x, $\bar{X}$	Molar fraction /Molar compound

Greek symbols

μ	Chemical potential
π	Local osmotic pressures of the solutions (MPa)
ϕ_η	Price modification coefficient in terms of efficiency
ϕ_T	Price modification coefficient in terms of temperature
ρ	Density (kg/m^3)
ΔT	Temperature difference (° C)
ΔT_{LM}	Logarithmic temperature (°C)
ΔP_{fb}	Pressure loss in the feed-brine water side of the membrane (kPa)
ΔP	Pressure loss (kPa)
η_{Ex}	Exergy efficiency (%)
η_T	Turbine efficiency
η_P	Pump efficiency
η_{IHE}	Internal Heat Exchanger efficiency
η_{th}	Thermal efficiency
T (p)	Temperature as a function of pressure
ε	Effectiveness
Ω	Non-dimensional function of the density difference between waste and the seawater in two modes of with and without preheating $\frac{(\rho_{15}-\rho_{sw})_{\text{Preheating}}}{(\rho_{15}-\rho_{sw})_{\text{Without; preheating}}}$.
$\bar{\Omega}$	Non-dimensional function percentage Ω

Subscripts

Atm	Atmosphere
App	Approach
B	Brine
BOF	Basic Oxygen Furnace
Ch	Chemical
Cond	Condenser
Cw	Cooling water
D	Destruction
Eco	Economizer

Eva	Evaporator
ERD	Energy recovery device
F	Fuel
F	Fluid
G	Gas
GWP	Global warming potential
g	Gas phase
HRSG	Heat recovery steam generator
HEX	Heat exchanger
IHE	Internal heat exchanger
i	Input
gen	Generation
max	Maximum
O	Output/outer
ODP	Ozone depletion potential
OFOH	Open feed-organic heater
ORC	Organic Rankine cycle side
P	Product/pump/permeate
ph	Physically
P.P	Pinch point
PV	Pressure vessels
Q	Heat
RO	Receive osmosis
SDI	Silt density index
SEC	Specific energy consumption
Sat	Saturated
Sw	Seawater
T	Turbine
TCF	Temperature correction factor
UPC	Unit product cost
W	Water/work/wall

$\langle...\rangle$	$\langle unit \rangle$
0	Reference environment condition
1,2, …,15	Stream number

CRediT authorship contribution statement

Declaration of competing interest

The authors declare that they have no known competing financial interests or personal relationships that could have appeared to influence the work reported in this paper.

Appendix. Determination of the parameters A_w and B from the DOW membranes.

The following equations are solved for the membrane, and the following inputs are extracted based on the standard test conditions of the membrane in the catalog: feed water density C_f, the water temperature, salt rejection (SR) rate, membrane area (S_m), recovery (R), and feed water pressure P_f.

By solving the salt balance ($Q_f \times C_f = Q_b \times C_b + Q_p \times C_p$) and SR ($SR = \frac{C_f - C_p}{C_f}$) equations simultaneously, the permeate density (C_p) and the density of salt in brine water (C_b) can be obtained (Mokhtari et al., 2016a):

$$C_p = C_f (1 - SR) \tag{A.1}$$

$$C_b = C_f \frac{(1 - R \times (1 - SR))}{1 - R} \tag{A.2}$$

The rate of the average density in the feed-water side of the membrane is determined by the formula (A.3) (Mokhtari et al., 2016a):

$$C_w = \frac{C_f}{2} \left(1 + \frac{C_b}{C_f} \right) \tag{A.3}$$

Utilizing the average density in feed-water brine side of the membrane and density polarization, the amount of the osmosis pressure average in the feed-water brine side of the membrane is calculated.

$$pf_i = \exp(0.7R) \tag{A.4}$$

$$\bar{\pi} = \pi_{C_f} \left(\frac{C_w}{C_s} \right) pf \tag{A.5}$$

In which pf $_i$ is the modified polarization density and the osmosis pressure in permeate side is also calculated from the following equation (Mokhtari et al., 2016a):

$$\bar{\pi}_{C_p} = \pi_f (1 - SR) \tag{A.6}$$

The amount of permeate mass flow rate is computed by (A.7) relation:

$$\dot{Q}_p = A_w(\bar{\pi})S_m(TCF)(FF)\left(P_f - \frac{\Delta P_{fb}}{2} - P_p - \bar{\pi} + \pi_{_{c_p}}\right) \tag{A.7}$$

P_p is the permeate pressure for each element and $A_w(\bar{\pi})$ is the permeability of the membrane for 'i' element in the temperature of 25 °C, which is the function of the osmosis pressure of the feed side and is calculated from Anon (0000b). In Eq. (A.7), S_m is the membrane area for each element obtained from the catalog and based on the type of the element. "FF" is the fouling factor, P_f is the feed pressure for each element, ΔP_{fb} is the pressure loss in the feed-brine water side of the membrane, and is calculated from Eq. (A.8).

$$\Delta P_{fb} = 0.01 n \bar{q}_{fb}^{1.7} \tag{A.8}$$

The pressure loss in the feed-brine water side of the membrane for each element of FILMTEC in the system is the function of the flow rate average in the feed side. It is calculated by the (A.9) formula:

$$\bar{q}_{fb} = \frac{\dot{Q}_f + \dot{Q}_b}{2} \tag{A.9}$$

The parameter "B" is calculated in terms of the reference Anon (0000b):

$$B = \frac{Q_p}{S_m} \frac{C_p}{C_w - C_p} \tag{A.10}$$

By calculating "B" and "A_w" coefficients for each membrane, the RO modeling is done according to the mentioned equations in Table 5 and the procedure of the reference Mokhtari et al. (2016a).

References

Abasi, M., Joorabian, M., Saffarian, A., Seifossadat, Seyyed Ghodratollah, 2020. A novel complete dynamic and static model of 48-pulse VSC-basedGUPFC for parallel transmission lines. Int. J. Ind. Electron. Control Optim. 3 (4), 447–457.

Al-Bastaki, N.M., Abbas, A., 2000. Predicting the performance of RO membranes. Desalination 132, 181–187, REFPROP version 7.1, NIST standard reference database 23. America: the U.S. Secretary of Commerce; 2003.

Aljundi, I.H., 2011. Effect of dry hydrocarbons and critical point temperature on the efficiencies of organic Rankine cycle. Renew. Energy 36, 1196–1202.

Alshawish, A.M., Eshtaiwi, S.M., Shojaeighadikolaei, A., Ghasemi, A., Ahmadi, R., 2020. Sensorless control for permanent magnet synchronous motor (PMSM) using a reduced order observer. In: 2020 IEEE Kansas Power and Energy Conference (KPEC). IEEE, pp. 1–5.

Ameri, M., Ahmadi, P., Hamidi, A., 2008. Energy, exergy and exergoeconomic analysis of a steam power plant: A case study. Int. J. Energy Res. 33, 499–512.

Ameri, M., Mokhtari, H., Bahrami, M., 2016. Energy, exergy, exergoeconomic and environmental (4E) optimization of a large steam power plant: a case stud. Iran J. Sci. Technol. 40, 11–20.

Ameri, M., Mokhtari, H., Mostafavi Sani, M., 2018. 4E analyses and multi-objective optimization of different fuels application for a large combined cycle power plant. Energy 156, 371–386.

Anon, 0000a. The Report of IRAN Steel General Studies, The IRAN National Steel Company, Y-NST0-G0-02-00-EC-GE-002.

Anon, 0000b. Dow Water Solutions FILMTEC^{TM} Reverse Osmosis Membranes Technical Manual. Available: www.dow.com.

ANSI/ASHRAE Standard 34-2007, 2007. Designation and Safety Classification of Refrigerants. American Society of Heating, Refrigerating and Air-Conditioning Engineers, Inc.

Arab Chadegania, E., Sharifishourabib, M., Hajiarab, F., 2018. Comprehensive assessment of a multi-generation system integrated with a desalination system: Modeling and analyzing. Energy Convers. Manage. 174, 20–32.

Astolfi, M., Romano, M.C., Bombarda, P., 2014a. Binary ORC (organic Rankine cycles) power plants for the exploitation of medium-low temperature geothermal sources Part A: thermo dynamic optimization. Energy 66, 423–434.

Astolfi, M., Romano, M.C., Bombarda, P., Macchi, E., 2014b. Binary ORC (Organic Rankine Cycles) power plants for the exploitation of medium-low temperature geothermal sources Part B: techno-economic optimization. Energy 66, 435–446.

Ayachi, F., Ksayer, E.B., Zoughaib, A., 2014. ORC optimization for medium grade heat recovery. Energy 68, 47–56.

Baccioli, A., Antonelli, M., Desideri, U., Grossi, A., 2018. Thermodynamic and economic analysis of the integration of Organic Rankine Cycle and Multi-Effect Distillation in waste-heat recovery applications. Energy 16, 456–469.

Badr, O., O'Callaghan, P.W., Probert, S.D., 1990. Rankine-cycle systems for harnessing power from low-grade energy sources. Appl. Energy 36, 263–292.

Bao, J., Zhang, R., Lin, Y., Zhang, N., Zhang, X., He, G., 2018a. Simultaneous optimization of system structure and working fluid for the three-stage condensation Rankine cycle utilizing LNG cold energy. Appl. Therm. Eng. 140, 120–130.

Bao, J., Zhang, R., Yuan, T., Zhang, X., Zhang, N., He, G., 2018b. A simultaneous approach to optimize the component and composition of zeotropic mixture for power generation systems. Energy Convers. Manage. 165, 354–362.

Behnama, P., Arefic, A., Shafii, M.B., 2018. Exergetic and thermoeconomic analysis of a trigeneration system producing electricity, hot water, and fresh water driven by low-temperature geothermal sources. Energy Convers. Manage. 157, 266–276.

Bejan, A., Moran, M.J., 1996. Thermal Design and Optimization. John Wiley & Sons.

Beni, M.H., Bazofti, M.M., Mohammadi, A.A., Golkar, B., H. Mokhtari, A.H., 2021. Water-energy nexus approach for optimal design of hybrid cooling system in direct reduction of iron plant. J. Cleaner Prod. 287, 125576.

Birnhack, L., Voutchkov, N., Lahav, O., 2011. Fundamental chemistry and engineering aspects of post-treatment processes for desalinated water—A review. Desalination 273, 6–22.

Borsukiewicz-Gozdur, A., Nowak, W., 2007. Comparative analysis of natural and synthetic refrigerants in application to low temperature Clausius-Rankine cycle. Energy 32, 344–352.

Branchini, L., Pascale, A.D., Peretto, A., 2013. Systematic comparison of ORC configurations by means of comprehensive performance indexes. Appl. Therm. Eng. 61, 129–140.

Bruno, J.C., López-Villada, J., Letelier, E., Romera, S., Coronas, Alberto, 2008. Modelling and optimisation of solar organic Rankine cycle engines for reverse osmosis desalination. Appl. Therm. Eng. 28, 2212–2226.

Cai, X., Shi, K., Zhong, S., Pang, X., 0000. Dissipative sampled-data control for high-speed train systems with quantized measurements. EEE Trans. Intell. Transp. Syst. PP(99), 1–12.

Camporeale, S.M., Pantaleo, A.M., Ciliberti, P.D., Fortunato, B., 2015. Cycle configuration analysis and techno-economic sensitivity of biomass externally fired gas turbine with bottoming ORC. Energy Convers. Manage. 105, 1239–1250.

Chammas, R., Clodic, D., 2005. Combined Cycle for Hybrid Vehicles. SAE Technical Paper, 01–1171.

Chao. K. Zhang, L., Li, Z., Zhu, Y., Wang, J., Yu, Z., 2018. Geographically weighted regression based methods for merging satellite and gauge precipitation. J. Hydrol. 558, 275–289.

Chen, Q., Xu, L., Chen, H., 2012. A new design method for Organic Rankine Cycles with constraint of inlet and outlet heat carrier fluid temperatures coupling with the heat source. Appl. Energy 98, 562–573.

Dai, Y., Wang, J., Gao, L., 2009. Parametric optimization and comparative study of organic Rankine cycle (ORC) for low grade waste heat recovery. Energy Convers. Manage. 50, 576–582.

Daryayehsalameh, B., Nabavi, M., Vaferi, B., 2021. Modeling of CO_2 capture ability of [Bmim][BF4] ionic liquid using connectionist smart paradigms. Environ. Technol. Innov. 22, 101484.

Davarpanah, A., 2018. Feasible analysis of reusing flowback produced water in the operational performances of oil reservoirs. Environ. Sci. Pollut. Res. 25 (35), 35387–35395.

Davarpanah, A., 2020. Parametric study of polymer-nanoparticles-assisted injectivity performance for axisymmetric two-phase flow in EOR processes. Nanomaterials 10 (9), 1818.

Davarpanah, A., Mirshekari, B., 2019. Experimental investigation and mathematical modeling of gas diffusivity by carbon dioxide and methane kinetic adsorption. Ind. Eng. Chem. Res. 58 (27), 12392–12400.

Delgado-Torres, A.M., García-Rodríguez, L., 2007a. Double cascade organic Rankine cycle for solar-driven reverse osmosis desalination. Desalination 216, 306–313.

Delgado-Torres, A.M., García-Rodríguez, L., 2007b. Preliminary assessment of solar organic Rankine cycles for driving a desalination system. Desalination 216, 252–275.

Delgado-Torres, A.M., García-Rodríguez, L., 2010. Preliminary design of seawater and brackish water reverse osmosis desalination systems driven by low-temperature solar organic Rankine cycles (ORC). Energy Convers. Manage. 51, 2913–2920.

Delgado-Torresa, A.M., Garcia-Rodriguez, L., 2012. Design recommendations for solar organic Rankine cycle (ORC)–powered reverse osmosis (RO) desalination. Renew. Sustain. Energy Rev. 16, 44–53.

Desai, N.B., Bandyopadhyay, S., 2009. Process integration of organic Rankine cycle. Energy 34, 1674–1686.

Doneker, R.L., Jirka, G.H., 2001. CORMIX-GI systems for mixing zone analysis of brine wastewater disposal. Desalination 139, 263–274.

Dong, S., Zhu, H., Zhong, S., Shi, K., Liu, Y., 2021. New study on fixed-time synchronization control of delayed inertial memristive neural networks. Appl. Math. Comput. 399, 126035.

Drescher, U., Brüggemann, D., 2007. Fluid selection for the Organic Rankine Cycle (ORC) in biomass power and heat plants. Appl. Therm. Eng. 27, 223–228.

Du, X., Qiu, J., Deng, S., Du, Z., Cheng, X., et al., 2021. Flame-retardant and solid–solid phase change composites based on dopamine-decorated BP nanosheets/Polyurethane for efficient solar-to-thermal energy storage. Renew. Energy 164, 1–10. https://doi.org/10.1016/j.renene.2020.09.067.

Du, Y., Xie, L., Liu, J., Wang, Y., Xu, Y., Wang, S., 2014. Multi-objective optimization of RO networks by lexicographic optimization and augmented epsilon constraint method. Desalination 333, 66–81.

Duan. B. Deng, X., Liu, Y., Li. J. Liu, Y., 2021. Experimental study the impacts of the key operating and design parameters on the cycle-to-cycle variations of the natural gas SI engine. Fuel 290, 119976.

Ehyaei, M.A., Ahmadi, A., Rosen, Marc A., Davarpanah, Afshin, 2020. Thermodynamic optimization of a geothermal power plant with a genetic algorithm in two stages. Processes 8 (10), 1277. https://doi.org/10.3390/pr8101277.

El-Emam, R.S., Dincer, I., 2018. Investigation and assessment of a novel solar-driven integrated energy system. Energy Convers. Manage. 158, 246–255.

Esfandi, S., Baloochzadeh, S., Asayesh, M., Ehyaei, M.A., Ahmadi, A., Arsalan Rabanian, A., Das, B., Costa, Vitor A.F., Davarpanah, A., 2020. Energy, exergy, economic, and exergoenvironmental analyses of a novel hybrid system to produce electricity, cooling, and syngas. Energies (13), 1–27.

Eveloy, V., Rodgers, P., Al Alili, A., 2017. Multi-objective optimization of a pressurized solid oxide fuel cell–gas turbine hybrid system integrated with seawater reverse osmosis. Energy 123, 594–614.

Façao, J., Palmero-Marrero, A., Oliveira, A.C., 2008. Analysis of a solar assisted micro-cogeneration ORC system. Int. J. Low-Carbon Technol. 3, 254.

Ganapathy, V., 2003. Industrial Boilers and Heat Recovery Steam Generators. Marcel Dekker.

Gao, C., Wang, D., Dong, H., Cai, J., Zhu, W., Du, T., 2011. Optimization and evaluation of steel enterprise's water-use system. J. Cleaner Prod. 19, 64–69.

García-Rodríguez, L., Delgado-Torres, A.M., 2007. Solar-powered Rankine cycles for fresh water production. Desalination 212, 319–327.

Geng, D., Du, Y., Yang, R., 2016. Performance analysis of an organic Rankine cycle for a reverse osmosis desalination system using zeotropic mixtures. Desalination 381, 38–46.

Green, S., 2020. A digital start-up project–carm tool as an innovative approach to digital government transformation. Comput. Syst. Sci. Eng. 35 (4), 257–269.

Gu, Y., Xu, J., Keller, A.A., Yuan, D., Li, Y., Zhang, B., Weng, Q., Zhang, X., Deng, P., Wang, H., Li, F., 2015. Calculation of water footprint of the iron and steel enterprise: A case study in eastern China. J. Cleaner Prod. 92, 274–281.

Guan, Q., Jiang, Y., 2020. An improved tcp vegas model for the space networks of the bandwidth asymmetry. Intell. Autom. Soft Comput. 26 (4), 773–781.

Han, Y., Li. H. Feng. Y. Tian. Z. Jiang. Tong He, H., 2021. Mechanism of dislocation evolution during plastic deformation of nitrogen-doped CoCrFeMnNi high-entropy alloy. Mater. Sci. Eng. A 814 (13), 141235.

Henthorne, L., Boysen, B., 2015. State-of-the-art of reverse osmosis desalination pretreatment. Desalination 356, 129–139.

Hettiarachchi, M., Golubovic, M., Worek, W., 2007. Optimum design criteria for an Organic Rankine cycle using low-temperature geothermal heat sources. Energy 32, 1698–1706.

Hou, C., Yin, M., Lan, P., Wang, H., Nie X. Ji, H., 2021. Recent progress in the research of angelica sinensis (oliv.) diels polysaccharides: extraction, purification, structure and bioactivities. Chem. Biol. Technol. Agric. 8, 13.

Hu, J., Wang, M., Zhao, C., Du, C., 2021. Formation control and collision avoidance for multi-UAV systems based on voronoi partition. Mech. Syst. Signal Process. 156, 107586.

Hu, J., Wang, M., Zhao, C., Pan, Q., Du, C., 2020a. Formation control and collision avoidance for multi-UAV systems based on voronoi partition. Sci. China Technol. Sci. 63, 65–72.

Hu, X., Xie, J., Cai, W., Wang, R., Davarpanah, A., 2020b. Thermodynamic effects of cycling carbon dioxide injectivity in shale reservoirs. J. Pet. Sci. Eng. 195, 107717.

Hu, J., Zhang, H., Li, Z., Zhao, C., Xu, Z., Pan, Q., 0000. Object traversing by monocular UAV in outdoor environment. Asian J. Control. http://dx.doi.org/10.1002/asjc.2415.

Hu, J., Zhang, H., Liu, L., Zhu, X., Zhao, C., Pan, Q., 2020c. Convergent multiagent formation control with collision avoidance. IEEE Trans. Robot. 36 (6), 1805–1818. https://doi.org/10.1109/TRO.2020.2998766.

Hua, L., Zhu, H., Shi, K., Zhong, S., Tang, Y., Liu, Y., 2021. Novel finite-time reliable control design for memristor-based inertial neural networks with mixed time-varying delays. IEEE Trans. Circuits Syst. I: Regular Papers 68 (4), 1599–1609. https://doi.org/10.1109/TCSI.2021.3052210.

Huang, S., 2020. The influence of digital multimedia communication forms on graphic design. Comput. Syst. Sci. Eng. 35 (3), 215–222.

Igobo, O.N., Davies, P.A., 2018. Isothermal Organic Rankine Cycle (ORC) driving Reverse Osmosis (RO) Desalination: experimental investigation and case study using R245fa working fluid. Appl. Therm. Eng. https://doi.org/10.1016/j.applthermaleng.2018.02.056.

Imran, M., Park, B.S., Kim, H.J., 2014. Thermo-economic optimization of Regenerative Organic Rankine Cycle for waste heat recovery applications. Energy Convers. Manage. 87, 107–118.

Jafarishiadeh, F., Mohammadi, F., 2020. M sahraei-ardakani preventive dispatch for transmission de-icing. IEEE Trans. Power Syst. 35 (5), 4104–4107.

Ji, X., Hou, C., Gao, Y., Xue, Y., Yan, Y., Guo, X., 0000. Metagenomic analysis of gut microbiota modulatory effects of jujube (Ziziphus jujuba Mill.) polysaccharides in a colorectal cancer mouse mode. Food Funct. https://doi.org/10.1039/C9FO02171J.

Ji, X., Hou, C., Shi, M., Liu, Y., 2020. An insight into the research concerning panax ginseng C. A. Meyer polysaccharides: A review. Food Rev. Int. 1–17. https://doi.org/10.1080/87559129.2020.1771363.

Ji, X., Peng, B., Ding, H., Cui, B., Nie, H., Yan, Y., 2021. Purification, structure and biological activity of pumpkin polysaccharides: A review. Food Rev. Int.

Jiang, J., M.ASCE, Peng, Z.Y., Ye, M., Wang, Y.B., 2021. Thermal effect of welding on mechanical behavior of high-strength steel. J. Mater. Civ. Eng. 33.

Jiang, Q., Shao, F., Lin, W., Gu, K., Jiang, G., et al., 2018. Optimizing multistage discriminative dictionaries for blind image quality assessment. IEEE Trans. Multimed. 20 (8), 2035–2048. https://doi.org/10.1109/TMM.2017.2763321.

Jung, Y., Kang, M., You, Y., 2020. Complexity effective frequency and sidelink synchronization algorithm for lte device-to-device communication systems. Comput. Mater. Contin. 62 (1), 443–458.

Karellas, S., Terzis, K., Manolakos, D., 2011. Investigation of an autonomous hybrid solar thermal ORC-PV RO desalination system. The Chalki Island case. Renew. Energy 36, 583–590.

Karimi, S., Mansouri, S., 2017. A comparative profitability study of geothermal electricity production in developed and developing countries: exergoeconomic analysis and optimization of different ORC configurations. Renew. Energy 115, 600–619.

Kasaeian, A., Nouri, G., Ranjbaran, P., Wen, D., 2018. Solar collectors and photovoltaics as combined heat and power systems: A critical review. Energy Convers. Manage. 156, 688–705.

Khanarmuei, M., Ahmadisedigh, H., Ebrahimi, I., Gosselin, L., Mokhtari, H., 2017. Comparative design of plug and recirculation RO systems; thermoeconomic: Case study. Energy 121, 205–219.

Kianfard, H., Khalilarya, S., Jafarmadar, S., 2018. Exergy and exergoeconomic evaluation of hydrogen and distilled water production via combination of PEM electrolyzer, RO desalination unit and geothermal driven dual fluid ORC. Energy Convers. Manage. 177, 339–349.

Kordestani, H., Zhang, C., Sami F. Masri, M.Shadabfar, 2021. An empirical time-domain trend line-based bridge signal decomposing algorithm using Savitzky–Golay filter. Struct. Control Health Monit. 28, 04–24.

Kosmadakis, G., Manolakos, D., Kyritsis, S., Papadakis, G., 2009a. Comparative thermodynamic study of refrigerants to select the best for use in the high-temperature stage of a two-stage organic Rankine cycle for RO desalination. Desalination 243, 74–94.

Kosmadakis, G., Manolakos, D., Kyritsis, S., Papadakis, G., 2009b. Economic assessment of a two-stage solar organic Rankine cycle for reverse osmosis desalination. Renew. Energy 34, 1579–1586.

Kosmadakis, G., Manolakos, D., Kyritsis, S., Papadakis, G., 2010a. Design of a two stage Organic Rankine Cycle system for reverse osmosis desalination supplied from a steady thermal source. Desalination 250, 323–328.

Kosmadakis, G., Manolakos, D., Papadakis, G., 2010b. Parametric theoretical study of a two-stage solar organic Rankine cycle for RO desalination. Renew. Energy 35, 989–996.

Ladewig, B., Asquith, B., 2012. Desalination Concentrate Management. Springer; Verlag Berlin Heidelberg.

Lai, X., Long, R., Liu, Z., Liu, W., 2018. Stirling engine powered reverse osmosis for brackish water desalination to utilize moderate temperature heat. Energy 165, 916–930.

Lemort, V., Cuevas, C., Lebrun, J., Teodorese, I.V., 2007. Contribution à l'étude des cycles de Rankine de récupération de chaleur. VIIIeme Colloque Interuniver-sitaire Franco-Quebecois sur la Thermique des Systemes. In: Presented at the VIIIème Colloque Interuniversitaire Franco-Québécois sur la Thermique des Systèmes Montreal.

Li, N., 2020. Construction and application of the multi-intermediate multi-media english oral teaching mode. Intell. Autom. Soft Comput. 26 (4), 807–815.

Li, C., Besarati, S., Goswami, Y., Stefanakos, E., Chen, H., 2013a. Reverse osmosis desalination driven by low temperature supercritical organic Rankine cycle. Appl. Energy 102, 1071–1080.

Li, C., Kosmadakis, G., Manolakos, D., Stefanakos, E., Papadakis, G., Goswami, D.Y., 2013b. Performance investigation of concentrating solar collectors coupled with a transcritical organic Rankine cycle for power and seawater desalination co-generation. Desalination 318, 107–117.

Li, Z., Li, W., Xu, B., 2016. Optimization of mixed working fluids for a novel trigeneration system based on organic Rankine cycle installed with heat pumps. Appl. Therm. Eng. 94, 754–762.

Li, Y., Wang, S., Xu, T., Li, J., Zhang, Y., Xu, T., et al., 2021. Novel designs for the reliability and safety of supercritical water oxidation process for sludge treatment. Process Saf. Environ. Prot. 149, 385–398. https://doi.org/10.1016/j.psep.2020.10.049.

Lingfeng Shia, A., Shua, G., Tiana, H., Deng, S., 2018. Review of modified Organic Rankine cycles (ORCs) for internal combustion engine waste heat recovery (ICE-WHR). Renew. Sustain. Energy Rev. 92, 95–110.

Liu, B., Chien, K., Wang, C., 2004. Effect of working fluids on organic Rankine cycle for waste heat recovery. Energy 29, 1207–1217.

Liu, X., Wei, M., Yang, L., Wang, X., 2017. Thermo-economic analysis and optimization selection of ORC system configurations for low temperature binary-cycle geothermal plant. Appl. Therm. Eng. 125, 153–164.

Liu, X., Zhang, B., Feng, Y., Lv, X., Ji, D., Niu, Z., Yang, Y., Zhao, X., Fan, Y., 2020. Development of 340-GHz transceiver front end based on GaAs monolithic integration technology for THz active imaging array. Appl. Sci. 10 (21), 7924.

Llor, A., 2005. Statistical Hydrodynamic Models for Developed Mixing Instability Flows_ Analytical "0D" Evaluation Criteria, and Comparison of Single-and Two-Phase. Springer, Berlin Heidelberg.

Loya-Fernández, Á., Ferrero-Vicente, L.M., Marco-Méndez, C., Martínez-García, E., Zubcoff, J., Sánchez-Lizaso, J.L., 2012. Comparing four mixing zone models with brine discharge measurements from a reverse osmosis desalination plant in Spain. Desalination 286, 217–224.

Lu, P., Li, H., Feng, H., Jiang, Z., Zhu, H., Liu, Z., He, T., 2021. Formation mechanism of AlN inclusion in high-nitrogen stainless bearing steels. Metall. Mater. Trans. B.

Lv, Z., Chen, D., Wang, Q., 2021. Diversified technologies in internet of vehicles under intelligent edge computing. IEEE Trans. Intell. Transp. Syst. 22 (4), 2048–2059.

Lv, Z., Lou, R., Singh, A.K., 0000. AI empowered communication systems for intelligent transportation systems. IEEE Trans. Intell. Transp. Syst. https://doi.org/10.1109/TITS.2020.3017183.

Ma, X., Zhang, K., Zhang, L., Yao, C., Yao, J., Wang, H., et al., 0000. Data-driven niching differential evolution with adaptive parameters control for history matching and uncertainty quantification. SPE J. 10-18. http://dx.doi.org/10.2118/205014-PA.

Macchi, E., Astolfi, M., 2016. Organic Rankine Cycle (ORC) Power Systems. Technologies and Applications. Woodhead Publishing.

Mago, P., Chamra, L.M., Srinivasan, K., Somayaji, C., 2008. An examination of regenerative organic Rankine cycles using dry fluids. Appl. Therm. Eng. 28, 998–1007.

Maizza, V., Maizza, A., 2001. Unconventional working fluids in organic Rankine-cycles for waste energy recovery systems. Appl. Therm. Eng. 21, 381–390.

Manolakos, D., Kosmadakis, G., Kyritsis, S., Papadakis, G., 2009a. Identification of behavior and evaluation of performance of small scale, low-temperature Organic Rankine Cycle system coupled with a RO desalination unit. Energy 34, 767–774.

Manolakos, D., Kosmadakis, G., Kyritsis, S., Papadakis, G., 2009b. On site experimental evaluation of a low-temperature solar organic Rankine cycle system for RO desalination. Sol. Energy 83, 646–656.

Manolakosa, D., Mohameda, E.Sh., Karagiannis, I., Papadakis, G., 2008. Technical and economic comparison between PV-RO system and RO-Solar Rankine system. Case study: Thirasia Island. Desalination 221, 37–46.

Manolakosa, D., Papadakisa, G., E.Sh., Mohameda, Kyritsisa, S., Bouzianas, K., 2005. Design of an autonomous low-temperature solar Rankine cycle system for reverse osmosis desalination. Desalination 183, 73–80.

Manolakosa, D., Papadakisa, G., Kyritsisa, S., Bouzianas, K., 2007. Experimental evaluation of an autonomous low-temperature solar Rankine cycle system for reverse osmosis desalination. Desalination 203, 366–374.

Mehrpooya, M., Ghorbani, B., Hossein, S.S., 2018. Thermodynamic and economic evaluation of a novel concentrated solar power system integrated with absorption refrigeration and desalination cycles. Energy Convers. Manage. 175, 337–356.

Mehrpooya, M., Ghorbani, B., Hossein, S.S., 2019. Developing and exergetic performance assessment of biogas upgrading process driven by flat plate solar collectors coupled with Kalina power cycle. Energy Convers. Manage. 181, 398–413.

Mikielewicz, D., Mikielewicz, J., 2010. A thermodynamic criterion for selection of working fluid for subcritical and supercritical domestic micro CHP. Appl. Therm. Eng. 30, 2357–2362.

Modesto, M., Nebra, S.A., 2009. Exergoeconomic analysis of the power generation system using blast furnace and coke oven gas in a Brazilian steel mill. Appl. Therm. Eng. 29, 2127–2136.

Mokhtari, H., Ahmadisedigh, H., Ameri, M., 2017. The optimal design and 4E analysis of double pressure HRSG utilizing steam injection for Damavand power plant. Energy 118, 399–413.

Mokhtari, H., Ahmadisedigh, H., Ebrahimi, I., 2016a. Comparative 4E analysis for solar desalinated water production by utilizing organic fluid and water. Desalination 377, 108–122.

Mokhtari, H., Esmaili, A., Hajabdollahi, H., 2016b. Thermo-economic analysis and multi-objective optimization of dual pressure combined cycle power plant with supplementary firing. Heat Transf. - Asian Res. 45, 59–84.

Mokhtari, H., Hadiannasab, H., Mostafavi, M., A. Ahmadibeni, B., 2016c. Determination of optimum geothermal Rankine cycle parameters utilizing coaxial heat exchanger. Energy 102, 260–275.

Mokhtari, H., Sepahv, M., fasihfar, A., 2016d. Thermoeconomic and exergy analysis in using hybrid systems (GT+MED+RO) for desalination of brackish water in Persian Gulf. Desalination 399, 1–15, https://www.icis.com.

Nabati, A.M., Sadeghi, M.S., Nikbakht Naserabad, S., Mokhtari, H., izadpanah, S., 2018. Thermo-economic analysis for determination of optimized connection between solar field and combined cycle power plant. Energy 162, 1062–1076.

Nafey, A.S., Sharaf, M.A., García-Rodríguez, L., 2010. Thermo-economic analysis of a combined solar organic Rankine cycle-reverse osmosis desalination process with different energy recovery configurations. Desalination 261, 138–147.

Nemati, A., Sadeghi, M., Yari, M., 2017. Exergoeconomic analysis and multi-objective optimization of a marine engine waste heat driven RO desalination system integrated with an organic Rankine cycle using zeotropic working fluid. Desalination 422, 113–123.

Ni, J., Zhuang, X., Wahab, M.A., 2020. Review on the prediction of residual stress in welded steel components. Comput. Mater. Contin. 62 (2), 495–523.

Niu, Z., Zhang, B., Wang, J., Liu, K., Chen, Z., Yang, K., Zhou, Z., Fan, Y., Zhang, Y., Ji, D., 2020. The research on 220 GHz multicarrier high-speed communication system. China Commun. 17 (3), 131–139.

Peñate, B., García-Rodríguez, L., 2012. Seawater reverse osmosis desalination driven by a solar Organic Rankine Cycle: Design and technology assessment for medium capacity range. Desalination 284, 86–91.

Peng, X., Liu, Z., Jiang, D., 2021. A review of multiphase energy conversion in wind power generation. Renew. Sustain. Energy Rev. 147, 111172.

Pethurajan, V., Sivan, S., Joy, G.C., 2018. Issues, comparisons, turbine selections and applications–An overview in organic Rankine cycle. Energy Convers. Manage. 166, 474–488.

Quader, M.A., Ahmed, S., Ghazilla, R.A.R., Ahmed, S., Dahari, M., 2015. A comprehensive review on energy efficient CO_2 breakthrough technologies for sustainable green iron and steel manufacturing. Renew. Sustain. Energy Rev. 50, 594–614.

Razmjoo, A., Kaigutha, L.G., Rad, M.V., Marzband, M., Davarpanah, A., Denai, M., 2020. A technical analysis investigating energy sustainability utilizing reliable renewable energy sources to reduce CO2 emissions in a high potential area. Renew. Energy.

Rostamijavanani, A., Ebrahimi, M.R., Jahedi, S., 2020. Thermal post-buckling analysis of laminated composite plates embedded with shape memory alloy fibers using semi-analytical finite strip method. J. Fail Anal. Prev. https://doi.org/10.1007/s11668-020-01068-5.

Rostamijavanani, A., Ebrahimi, M.R., Jahedi, S., 2021. Free vibration analysis of composite structures using semi-analytical finite strip method. J. Fail. Anal. Prev. https://doi.org/10.1007/s11668-021-01136-4.

Roy, J.P., Mishra, M.K., Misra, A., 2011. Performance analysis of an Organic Rankine Cycle with superheating under different heat source temperature conditions. Appl. Energy 88, 2995–3004.

Sadeghi, M., Nemati, A., Ghavimi, A., Yari, M., 2016. Thermodynamic analysis and multi-objective optimization of various ORC (organic Rankine cycle) configurations using zeotropic mixtures. Energy 109, 791–802.

Safarian, S., Aramoun, F., 2015. Energy and exergy assessments of modified organic Rankine Cycles (ORCs). Energy Rep. 1, 1–7.

Saleh, B., Koglbauer, G., Wendl, M., Fischer, J., 2007. Working fluids for low-temperature organic Rankine cycles. Energy 32, 1210–1221.

Salimi, M., Amidpour, M., 2017. Modeling, simulation, parametric study and economic assessment of reciprocating internal combustion engine integrated with multi-effect desalination unit. Energy Convers. Manage. 138, 299–311.

Sayyaadi, H., Mehrabipour, R., 2012. Efficiency enhancement of a gas turbine cycle using an optimized tubular recuperative heat exchanger. Energy 38, 362–375.

Sharqawy, M.H., Lienhard, J.H., Zubair, S.M., 2011. On exergy calculations of seawater with applications in desalination systems. Int. J. Therm. Sci. 50, 187–196.

Shayesteh, A.A., Koohshekan, O., Ghasemi, A., Nemati, M., Mokhtari, H., 2019. Determination of the ORC-RO system optimum parameters based on 4E analysis; Water–Energy-Environment nexus. Energy Convers. Manage. 183, 772–790.

Shirmohammadi, R., Aslani, A., Ghasempour, R., 2020a. Challenges of carbon capture technologies deployment in developing countries. Sustain. Energy Technol. Assess. 42, 100837.

Shirmohammadi, R., Aslani, A., Ghasempour, R., Romeo, L.M., 2020b. CO_2 utilization via integration of an industrial post-combustion capture process with a urea plant: Process modelling and sensitivity analysis. Processes 8 (9), 1144.

Song, S., Choi, M., Goh, Y., Yun, J., Yoo, W., et al., 2020. Analysis of wireless backhaul networks based on aerial platform technology for 6g systems. Comput. Mater. Contin. 62 (2), 473–494.

Song, J., Gu, C.W., 2015. Analysis of ORC (Organic Rankine Cycle) systems with pure hydrocarbons and mixtures of hydrocarbon and retardant for engine waste heat recovery. Appl. Therm. Eng. 89, 693–702.

Sun, L., Li, C., Zhang, C., Ti. Liang, Zhao, Z., 2019a. The strain transfer mechanism of fiber bragg grating sensor for extra large strain monitoring. Sensors 19 (8), 1851. https://doi.org/10.3390/s19081851.

Sun, M., Yan, L., Zhang, L., Song, L., Guo, J., et al., 2019b. New insights into the rapid formation of initial membrane fouling after in-situ cleaning in a membrane bioreactor. Process Biochem. (1991) 78, 108–113. https://doi.org/10.1016/j.procbio.2019.01.004.

Tang, P., Wang, Y., Shen, N., 2020. Prediction of college students' physical fitness based on k-means clustering and SVR. Comput. Syst. Sci. Eng. 35 (4), 237–246.

Tchanche, B.F., Lambrinos, Gr., Frangoudakis, A., Papadakis, G., 2010. Exergy analysis of micro-organic Rankine power cycles for a small scale solar driven reverse osmosis desalination system. Appl. Energy 87, 1295–1306.

Tchanche, B.F., Papadakis, G., Lambrinos, G., Frangoudakis, A., 2009. Fluid selection for a low-temperature solar organic Rankine cycle. Appl. Therm. Eng. 29, 2468–2476.

Vaja, I., Gambarotta, A., 2010. Internal Combustion Engine (ICE) bottoming with Organic Rankine Cycles (ORCs). Energy 35, 1084–1093.

Venkateshkumar, U., Ramakrishnan, S., 2020. Detection of the spectrum hole from n-number of primary users using the gencluster algorithm. Intell. Autom. Soft Comput. 26 (4), 817–830.

Vivian, J., Manente, G., Lazzaretto, A., 2015. A general framework to select working fluid and configuration of ORCs for low-to-medium temperature heat sources. Appl. Energy 156, 727–746.

Voutchkov, N., 2011. Overview of seawater concentrate disposal alternatives. Desalination 273, 205–219.

Wang, X., Jing, S., 2020. The construction and path analysis of the school-enterprise cooperative innovation model under the background of the open independent innovation. Intell. Autom. Soft Comput. 26 (4), 765–771.

Wang, N., Sun, X., Zhao, Q., Wang, P., 2021. Treatment of polymer-flooding wastewater by a modified coal fly ash-catalysed Fenton-like process with microwave pre-enhancement: System parameters, kinetics, and proposed mechanism. Chem. Eng. J. (Lausanne, Switzerland : 1996) 406, 126734. https://doi.org/10.1016/j.cej.2020.126734.

Wang, N., Sun, X., Zhao, Q., Yang, Y., Wang, P., 2020. Leachability and adverse effects of coal fly ash: A review. J. Hard Mater. 396, 122725. https://doi.org/10.1016/j.jhazmat.2020.122725.

Wang, M., Wang, J.F., Zhao, Y.Z., Zhao, P., Dai, Y.P., 2013a. Thermodynamic analysis and optimization of a solar-driven regenerative organic Rankine cycle (ORC) based on flat-plate solar collectors. Appl. Therm. Eng. 50, 816–825.

Wang, J.F., Yan, Z.Q., Wang, M., 2013b. Multi-objective optimization of an organic Rankine cycle (ORC) for low grade waste heat recovery using evolutionary algorithm. Energy Convers. Manage. 71, 146–158.

Wang, J.F., Yan, Z.Q., Wang, M., Ma, S.L., Dai, Y.P., 2013. Thermodynamic analysis and optimization of an (organic Rankine cycle) ORC using low grade heat source. Energy 49, 356–365.

Wang, E.H., Zhang, H.G., Fan, B.Y., Quyang, M.G., Zhao, Y., Mu, Q.H., 2011. Study of working fluid selection of organic Rankine cycle (ORC) for engine waste heat recovery. Energy 36, 3406–3418.

Wei, D., Lu, X., Lu, Z., Gu, J., 2007. Performance analysis and optimization of organic Rankine Cycle (ORC) for waste heat recovery. Energy Convers. Manage. 48, 1113–1119.

Xu, Q., Zou, Z., Chen, Y., Wang, K., Du, Z., Feng, J., et al., 2020. Performance of a novel-type of heat flue in a coke oven based on high-temperature and low-oxygen diffusion combustion technology. Fuel (Guildford) 267 (C), 117160. https://doi.org/10.1016/j.fuel.2020.117160.

Xue, X., Zhang, K., Tan, K.C., Feng, L., Wang, J., Chen, G., et al., 2020. Affine transformation-enhanced multifactorial optimization for heterogeneous problems. IEEE Trans. Cybern. PP, 1–15. https://doi.org/10.1109/TCYB.2020.3036393.

Yang, S., Li, Z., Yan, K., Zhang, X., Xu, Z., Liu, W., Liu, Z., Liu, H., 2021. Removing and recycling mercury from scrubbing solution produced in wet nonferrous metal smelting flue gas purification process. J. Environ. Sci..

Yang, Y., Li, Y., Yao, J., Iglauer, S., Luquot, L., Zhang, K., et al., 2020a. Dynamic pore-scale dissolution by CO2-saturated brine in carbonates: Impact of homogeneous versus fractured versus vuggy pore structure. Water Resour. Res. 56 (4), https://doi.org/10.1029/2019WR026112.

Yang, Y., Tao, L., Yang, H., Iglauer, S., Wang, X., Askari, R., et al., 2020b. Stress sensitivity of fractured and vuggy carbonate: An X-ray computed tomography analysis. J. Geophys. Res. Solid Earth 125 (3), https://doi.org/10.1029/2019JB018759.

Yang, Z., Xu, P., Wei, W., Gao, G., Zhou, N., et al., 2020c. Influence of the crosswind on the pantograph arcing dynamics. IEEE Trans. Plasma Sci. 48 (8), 2822–2830. https://doi.org/10.1109/TPS.2020.3010553.

Yang, Y., Yao, J., Wang, C., Gao, Y., Zhang, Q., An, S., et al., 2015. New pore space characterization method of shale matrix formation by considering organic and inorganic pores. J. Natural Gas Sci. Eng. 27, 496–503. https://doi.org/10.1016/j.jngse.2015.08.017.

Yang, M.H., Yeh, R.H., 2015. Thermo-economic optimization of an organic Rankine cycle system for large marine diesel engine waste heat recovery. Energy 82, 256–268.

Yao, H., Sheng, D., Chen, J., Li, W., Wan, A., Chen, H., 2013. Exergoeconomic analysis of a combined cycle system utilizing associated gases from steel production process based on structural theory of thermoeconomics. Appl. Therm. Eng. 51, 476–489.

Yoon, B., Ahn, Y., 2021. Effect of mo addition on aging behavior of TRIP-aided duplex stainless steel. Mater. Charact..

Yoon, H., Kim, K., Chun, J., 2020. Shadow detection and removal from photo-realistic synthetic urban image using deep learning. Comput. Mater. Contin. 62 (1), 459–472.

Yousefizadeh Dibazar, S., Salehi, Gh., Davarpanah, A., 2020. Comparison of exergy and advanced exergy analysis in three different organic Rankine cycles. Processes 8 (5), 586. https://doi.org/10.3390/pr8050586.

Yu, B., 2021. Urban spatial structure and total-factor energy efficiency in chinese provinces. Ecol. Indic. 126, 107662.

Zare, V., 2015. A comparative exergoeconomic analysis of different ORC configurations for binary geothermal power plants. Energy Convers. Manage. 105, 127–138.

Zhang, H., Guan, W., Zhang, L., Guan, X., Wang, S., 2020a. Degradation of an organic dye by bisulfite catalytically activated with iron manganese oxides: The role of superoxide radicals. ACS Omega 5 (29), 18007–18012. https://doi.org/10.1021/acsomega.0c01257.

Zhang, B., Ji, D., Fang, D., Liang, S., Fan, Y., Chen, X., 2019a. A novel 220-GHz gan diode on-chip tripler with high driven power. IEEE Electron Device Lett. 40 (5), 780–783.

Zhang, C., Jin, Q., Song, Y., Wang, J., Sun, L., Liu, H., Dun, L., Tai, H., Yuan, X., Xiao, H., Zhu, L., Guo, S., 0000. Vibration analysis of a sandwich cylindrical shell in hygrothermal environment, https://doi.org/10.1515/ntrev-2021-0026.

Zhang, B., Niu, Z., Wang, J., Ji, D., Zhou, T., Liu, Y., Feng, Y., Hu, Y., Zhang, J., Fan, Y., 2020b. Four-hundred gigahertz broadband multi-branch waveguide coupler. 14, (11), pp. 1175–1179.

Zhang, H., Sun, M., Song, L., Guo, J., Zhang, L., 2019b. Fate of NaClO and membrane foulants during in-situ cleaning of membrane bioreactors: Combined effect on thermodynamic properties of sludge. Biochem. Eng. J. 147, 146–152. https://doi.org/10.1016/j.bej.2019.04.016.

Zhang, K., Wang, Q., Chao, L., Ji, Ye, Li, Z., Yu, Z., Yang, T., Ju, Q., 2019c. Ground observation-based analysis of soil moisture spatiotemporal variability across a humid to semi-humid transitional zone in China. J. Hydrol. 574, 903–914.

Zhang, T., Wu, X., Shaheen, S.M., Rinklebe, J., Bolan, N.S., Ali, E.F., Li, G., Tsang, D.C.W., 0000. Effects of microorganism-mediated inoculants on humification processes and phosphorus dynamics during the aerobic composting of swine manure. https://doi.org/10.1016/j.jhazmat.2021.125738.

Zhang, Y., Xia, X., Wu, Z., Zhang, Q., 2020c. The effect of initial defects on overall mechanical properties of concrete material. Comput. Mater. Contin. 62 (1), 413–442.

Zhang, K., Zhang, J., Ma, X., Yao, C., Zhang, L., Yang, Y., et al., 2021. History matching of naturally fractured reservoirs using a deep sparse autoencoder. SPE J. 1–22. https://doi.org/10.2118/205340-PA.

Zhang, R., Zhao, X., 2020. The application of folk art with virtual reality technology in visual communication. Intell. Autom. Soft Comput. 26 (4), 783–793.

Zhang, X., Zhou, S., Fang, J., Ni, Y., 2020d. Pattern recognition of construction bidding system based on image processing. Comput. Syst. Sci. Eng. 35 (4), 247–256.

Zhu, G., Liu, W., Zhang, S., Chen, X., Yin, C., 2020. The method for extracting new login sentiment words from chinese micro-blog basedf on improved mutual information. Comput. Syst. Sci. Eng. 35 (3), 223–232.

Zuo, C., Chen, Q., Tian, L., Waller, L., Asundi, A., 2015. Transport of intensity phase retrieval and computational imaging for partially coherent fields: The phase space perspective. Opt. Lasers Eng. 71, 20–32. https://doi.org/10.1016/j.optlaseng.2015.03.006.

Zuo, C., Sun, J., Li, J., Zhang, J., Asundi, A., et al., 2017. High-resolution transport-of-intensity quantitative phase microscopy with annular illumination. Sci. Rep. 7 (1), 7622–7654. https://doi.org/10.1038/s41598-017-06837-1.